Si Isotope Variability in Proterozoic Cherts

Si isotope variability in Proterozoic cherts

Ramananda Chakrabarti[1*#], Andrew H. Knoll[1, 2], Stein B. Jacobsen[1], Woodward W. Fischer[3]

1. Department of Earth and Planetary Sciences, Harvard University, Cambridge, MA 02138
2. Department of Organismic and Evolutionary Biology, Harvard University, Cambridge, MA 02138
3. Division of Geological and Planetary Sciences, California Institute of Technology, Pasadena, CA 91125

* Corresponding author # Present address: Center for Earth Sciences, Indian Institute of Science, Bangalore, Karnataka 560 012, India (ramananda@ceas.iisc.ernet.in; ramananda@gmail.com; Tel: +91-80-2293-3003)

Emails:
Ramananda Chakrabarti (ramananda@gmail.com; ramananda@ceas.iisc.ernet.in)
Andrew H. Knoll (aknoll@oeb.harvard.edu)
Stein B. Jacobsen (jacobsen@neodymium.harvard.edu)
Woodward W. Fischer (wfischer@caltech.edu)

Abstract

We report Si-isotopic compositions of 75 sedimentologically and petrographically characterized chert samples with ages ranging from ~2600 to 750 Ma using multi-collector inductively coupled plasma mass spectrometry. δ^{30}Si values of the cherts analyzed in this study show a ~ 7‰ range, from -4.29 to +2.85. This variability can be explained in part by 1) simple mixing of silica derived from continental (higher δ^{30}Si) and hydrothermal (lower δ^{30}Si) sources, 2) multiple mechanisms of silica precipitation and 3) Rayleigh-type fractionations within pore waters of individual basins.

We observe ~3 ‰ variation in peritidal cherts from a single Neoproterozoic sedimentary basin (Spitsbergen). This variation can be explained by Rayleigh-type fractionation during precipitation from silica-saturated porewaters. In some samples, post-dissolution and reprecipitation of silica could have added to this effect. Our data also indicate that peritidal cherts are enriched in the heavier isotopes of Si whereas basinal cherts associated with banded iron formations (BIF) show lower δ^{30}Si. This difference could partly be due to Si being derived from hydrothermal sources in BIFs. We postulate that the difference in δ^{30}Si between non-BIF and BIF cherts isconsistent with the contrasting genesis of these deposits. Low δ^{30}Si in BIF is consistent with laboratory experiments showing that silica adsorbed onto Fe-hydroxide particles preferentially incorporates lighter Si isotopes.

Despite large intrabasinal variation and environmental differences, the data show a clear pattern of secular variation. Low δ^{30}Si in Archean cherts is consistent with a dominantly hydrothermal source of silica to the oceans at that time. The monotonically increasing δ^{30}Si from 3.8 Ga to 1.5 Ga appears to reflect a general increase in continental versus hydrothermal sources of Si in seawater, as well as the preferential removal of lighter Si isotopes during silica precipitation in iron-associated cherts from silica-saturated seawater. The highest δ^{30}Si values are observed in 1.5 Ga peritidal cherts; in part, these enriched values could reflect increasing sequestration of light silica during soil-forming processes, thus, delivering relatively heavy dissolved silica to the oceans from continental sources. The causes behind the reversal in trend towards lower δ^{30}Si in cherts younger than 1.5 Ga old are less clear. Cherts deposited 1800-1900 Ma are

especially low δ^{30}Si, a possible indication of transiently strong hydrothermal input at this time.

1. INTRODUCTION

Cherts, deposits of amorphous silica now microcrystalline quartz, are ubiquitous in the sedimentary rock record, documenting the evolution of the global silica cycle through geologic time (Maliva et al., 1989; Maliva et al., 2005). The isotopic composition of Si in Archean and Proterozoic cherts can provide insights into the sources and sinks of marine silica before the evolution of silica-precipitating sponges, radiolarians and diatoms. However, the use of sedimentary silica as a direct proxy for the composition and physical state of Precambrian seawater has limitations because most Precambrian cherts formed during the diagenesis of precursor sediments. Robert and Chaussidon (2006) measured the Si isotopic composition of an extensive set of chert samples, primarily from Archean and Proterozoic successions, but also including Phanerozoic examples, using an ion-microprobe technique. They interpreted their combined O and Si isotope data from Precambrian cherts to reflect seawater paleo-temperatures. Subsequent studies have highlighted the importance of the source of Si in determining the isotopic composition of preserved cherts (Steinhoefel et al., 2009; van den Boorn et al., 2007, 2010; Heck et al., 2011).

Improvements in mass spectrometry techniques, particularly multi-collector inductively coupled plasma mass spectrometry (MC-ICPMS), now permit Si isotopes to be measured with much better precision (2σ errors better than 0.1‰; e.g. Georg et al., 2006b; Chakrabarti and Jacobsen, 2010). MC-ICPMS Si isotope data are also accurate to better than 0.1 ‰ based on measurements of inter-laboratory standards.MC-SIMS allows sampling in high resolution but is limited to a 2σ uncertainty of 0.3 ‰ for δ^{30}Si (Heck et al., 2011) which, although a significant improvement compared to earlier ion-probe studies (e.g. Robert and Chaussidon, 2006; Basile-Doelsch et al., 2005) is still 3 times less precise than MC-ICPMS. Several recent studies have reported high-precision MC-ICPMS Si isotope measurements of cherts, primarily from Archean successions (Abraham et al., 2011; Andre et al., 2006; Steinhoefel et al., 2009, 2010; van den Boorn

et al., 2007, 2010). Here we report high-precision MC-ICPMS Si isotope data for a suite of well-characterized chert samples with ages ranging from ~2530 to ~750 Ma.

In the following sections we compare and contrast the modern and Precambrian silica cycles and interpret our Si isotope measurements of Late Archean and Proterozoic cherts based on the source of silica, mechanism of silica precipitation and depositional setting. The data document both marked isotopic variation within individual Proterozoic basins and, despite this, a clear pattern of change throughout the Proterozoic Eon, as originally observed by Robert and Chaussidon (2006). Along with previously available Si-isotopic measurements, our new data allow us to evaluate various mechanisms proposed to explain observed temporal variations in the Si isotopic composition of Precambrian cherts.

2. SAMPLES

We determined the Si-isotopic compositions of 75 chert samples with ages ranging from ~2600 to 750 Ma (Table 1). The samples come from measured sections and are well characterized sedimentologically and petrographically (see Table 1 for references and Fig. 1). They include peritidal cherts, which are largely early diagenetic replacements of precursor carbonate sediments, as well as basinal cherts, associated primarily with iron formation, deposited in environments up to several hundred meters below the sea surface. Our sample choice reflects two mutually reinforcing strategies.

In the first instance, given the range of δ^{30}Si values reported by Robert and Chaussidon (2006), we wanted to gauge the degree of isotopic variation within a single basin. Thus, we analyzed 21 samples from the ca. 800-720 Ma Akademikerbreen Group, Spitsbergen, and 3 samples from its correlatives on Nordaustlandet (Knoll, 1984) and in East Greenland (Green et al., 1989). This ca. 2000 m succession contains a variety of shallow marine carbonate facies, including tidal flat and lagoonal carbonates, oolites, and stromatolitic bioherms (Knoll and Swett, 1990). Cherts occur throughout the succession as irregular to ellipsoidal nodules as well as individually silicified ooids, microbial mat laminae, and thin flakes ripped up and redeposited in lagoons (Knoll et al., 1989). Field and petrographic observations indicate that the silica replaced original carbonate

sediments early in diagenesis (Maliva et al., 1989), a conclusion corroborated by the common occurrence of exceptionally well preserved microfossils in Akademikerbreen cherts (Knoll, 1985; Knoll, 1984; Knoll et al., 1989; Knoll et al., 1991). Indeed, the exceptional preservation of organic walled microfossils required the chert have been emplaced on the timescale of organic decay, no greater than a few thousand years after deposition and probably much less. Most of the cherts occur in coastal carbonates; this environmental dependence is expected for early oceans without silica biomineralizing protists and animals (Maliva et al., 1989). Finally, we also analyzed a pair of samples from the age-equivalent Fifteenmile Group (formerly assigned to the Lower Tindir Group), northwestern Canada (Allison and Awramik, 1989; Macdonald et al., 2010, 2011).

Our second strategy focused on the older end of the age spectrum. In the chert dataset of Robert and Chaussidon (2006), all samples, although screened for alteration using oxygen isotopes, are viewed as equivalent, in the sense that all were deemed equally likely to preserve a record of seawater Si-isotopic composition. However, it is clear from the sedimentary geology and petrography that these materials vary in mode of formation and environmental setting, raising the question of whether long term trends might principally reflect the succession in sample dominance from hydrothermal cherts in the Early Archean, to iron formation in late Archean and Paleoproterozoic basins, to pertidal cherts in younger Proterozoic basins (e.g. Fischer and Knoll, 2009; van den Boorn et al., 2010). Added to this is the potentially complicating issue that isotope fractionation accompanies silica adsorption onto iron oxides, with the lighter isotope preferentially enriched in the precipitate (Delstanche et al., 2009; Opfergelt et al., 2009). Thus, we analyzed 12 chert samples from the late Archean Transvaal Supergroup, South Africa (Knoll and Beukes, 2009), a collection that includes peritidal cherts in carbonates, deep water chert nodules and basinal iron formation. This allows us to ask whether the basinal sedimentation of silica adsorbed onto iron ferrihydroxides (e.g., Fischer and Knoll, 2009) imparts a detectable environmental variation onto cherts from this basin. Building on this, we also analyzed a pair of samples from the Late Archean Hamersley Supergroup, Australia (Yi-Liang et al., 2011), and eight samples from several 1800-1990

Ma successions that include late Paleoproterozoic iron formation (Barghoorn and Tyler, 1965; Tobin, 1990; Brotton et al., 2007; Wilson et al., 2010 and references therein).

Finally, to connect our Paleo- and Neoproterozoic sample sets, we analyzed silica nodules in pertidal carbonates from the ca. 1000-1100 Ma Sukhaya Tunguska Formation, northwestern Siberia (Sergeev et al., 1997, and references therein), the ca. 1200 Ma Narssarssuk Formation, northwestern Greenland, and correlative beds of the Society Cliffs, Formation, Baffin Island (Dawes, 1997; Kah and Knoll, 1996; Strother et al., 1983) and the 1400-1500 Ma Billyakh Group, northern Siberia (Sergeev et al., 1995). Petrographic similarities among all younger Proterozoic samples and their common preservation of microfossils suggest that all of these samples are similar in depositional setting, timing of formation, and mode of emplacement.

In addition to the above-mentioned chert samples, three inter-laboratory Si isotope ratio standards IRMM-018, Diatomite, and Big Batch (Reynolds et al., 2007), two in-house pure silicon standards from Alfa Aesar (Harvard-AA-Si) and High Purity Standards (Harvard-HPS-Si) as well as terrestrial mantle-derived igneous rocks from different tectonic settings including USGS standards BCR-1 (Columbia River basalt, Bridal Veil Flow Quarry) and BHVO-1 (basalt from Halemaumau, Hawaii) were also analyzed during this study. The results for the standards and silicate igneous rocks and minerals have been reported elsewhere (Chakrabarti and Jacobsen, 2010).

3. ANALYTICAL METHODS

Hand specimen-sized samples (~ 2 cubic inch) were coarsely crushed using a rock hammer. After crushing, rock chips were visually inspected for surface alteration and stains. Centimeter-size rock chips were cleaned with water in an ultrasonic bath, air-dried and subsequently crushed using an alumina mortar and pestle. Relatively large quantities of rock chips (~0.5-1 gm) were crushed to powder to obtain a homogeneous representation of each sample. For isotopic analysis, ~5 mg of rock powder was dissolved.

For this study, a HF acid-free dissolution technique was used, similar to published techniques (Georg et al., 2006b; van den Boorn et al., 2006; Chakrabarti and Jacobsen,

2010). About 5 mg of powdered sample was mixed with 150-200 mg of ultra-pure solid sodium hydroxide (NaOH) and 50 μl of 18 MΩ water in 5 ml in-house made Teflon containers which were tightly placed in custom-made stainless steel jackets and heated to ~200^{0}C in an oven for 72 hours. After dissolution, samples were transferred in ~100 ml of 0.05N HNO_3. Si was separated by ion-exchange chromatography using 2ml of the Bio-Rad 50W-x12 (200-400 mesh, H^+ form) cation exchange resin (Georg et al., 2006b). Si was eluted with 4-6 ml water and the Si yield was >99% for all samples.

Si isotopes (masses 28, 29 and 30) were analyzed using a GV IsoProbe-P Multi-Collector Inductively Coupled Plasma Mass Spectrometer (MC-ICPMS) at Harvard University in high resolution mode with a resolving power ($R_{power,\ 5\%-95\%}$) (Weyer and Schwieters, 2003) of 5000 and using an optimized proportion of H_2, He and Ar in the collision cell of the IsoProbe-P as described previously in Chakrabarti and Jacobsen (2010). We were able to resolve the $^{14}N_2H^+$ and $^{14}N^{16}O^+$ interferences on masses 29 and 30, respectively, and did not observe any interference on mass 28. All our samples and standards lie on a mass-dependent fractionation line which indicates that using high-resolution slits and collision cell gases, we were able to resolve all the potential isobaric interferences on the three isotopes of Si (see Chakrabarti and Jacobsen, 2010 for details). A sample-standard bracketing technique using NBS28 as the standard was used to correct for instrumental mass fractionation. NBS28, a pure quartz sand, was also dissolved and processed through chemistry in the same way as the samples. For all samples and the bracketing standard, we ran 5 ppm solutions which resulted in a ~4 volt signal on mass 28. Si concentration of the bracketing standard and sample was matched to within 10%. Total Si blanks in 1% v/v nitric acid was less than 1 mv. Hence, blank correction was not necessary.

Sample and standard solutions were introduced into the plasma using a spray chamber with heating and cooling options (APEX-IR, from Elemental Scientific Inc.) attached with a self-aspirating Teflon nebulizer (ESI) with an uptake rate of 100 μl/ minute. Si isotope ratio measurements were done in static mode involving a defocused ($\pm$ 0.5 mass) baseline measurement at the beginning of each analysis. Data were collected in one block of 25 cycles, each with an integration time of 10 seconds per cycle. Data reduction was performed off-line. Delta values were determined as δ^{xx}Si (‰) =

$[(^{xx}Si/^{28}Si)_{sample} / (^{xx}Si/^{28}Si)_{NBS28}) -1] \times 1000$ where xx is either mass 29 or 30. Long-term external reproducibility of our measurements is based on repeated measurements of Si standards over 2 years and is better than 0.05 ‰ ($2\sigma_m$, standard error of the mean) for $\delta^{30}Si$ (Chakrabarti and Jacobsen, 2010).

4. RESULTS

Our Si isotopic data for the chert samples are listed in Table 1. External reproducibility is reported as $2\sigma_m$. Results of our long term measurements of the inter-laboratory standards (Diatomite, IRMM-018 and Big Batch) obtained during the course of this study have been published elsewhere (Chakrabarti and Jacobsen, 2010) and agree with recommended values (Reynolds et al., 2007). All the above standards were processed in the same way as the samples, using ion-exchange chromatography. During the course of this study, we also analyzed two in-house pure silicon standards (Chakrabarti and Jacobsen, 2010) from Alfa Aesar (Harvard-AA-Si) and High Purity Solutions (Harvard-HPS-Si) with wide-ranging $\delta^{30}Si$ of -12.62 $\pm$ 0.02 and -0.81 $\pm$ 0.03, respectively (Chakrabarti and Jacobsen, 2010). Si isotopic compositions of the chemically purified aliquots of these pure Si standards are indistinguishable from those of the unprocessed pure Si solutions, validating the accuracy of our measurements for samples processed through chemical separation.

The $\delta^{30}Si$ values of the cherts analyzed in this study show a ~7‰ range, from -4.29 to +2.85. Three principal patterns require explanation. First, the samples show substantial variation (3-4‰) within both individual basins and time intervals. Second, despite this variation, there is a distinct pattern of secular change in Si-isotope ratios, from low $\delta^{30}Si$ values in early Archean (data from literature), which increases to a maximum (up to 2.85) in mid-Proterozoic cherts, after which $\delta^{30}Si$ values decline toward the present (Figure 2, the inferred average trend during the Precambrian is shown schematically as a yellow band). Against this backdrop, values for successions that contain iron formation stand out for their relatively low $\delta^{30}Si$ values (+0.57 to -4.29), particularly those from ca. 1.8-1.9 Ga ($\delta^{30}Si$ = -1.57 to -4.29), with extremely low values in two samples from the Frere and Duck Creek formations.

5. DISCUSSION

5.1. Si cycling and Si isotopes in the modern Earth system

Continental weathering is the dominant source of silicic acid to the modern oceans, delivered primarily as dissolved load in river waters (Treguer et al., 1995) (Table 2) as well as groundwater fluxes (Georg et al., 2009). Although the flux of suspended silica-rich particles in rivers is greater than the dissolved silicic acid (H_4SiO_4) flux, further dissolution of this particulate matter is slow and its contribution to the silicic acid flux to the oceans is negligible (Treguer et al., 1995). Other silica sources include hydrothermal fluids and seafloor weathering of basalts. Biogenic uptake of dissolved silica constitutes the major sink for silicic acid in the modern oceans and the estimated output balances the input (Table 2). Silica is undersaturated in modern oceans, with an average concentration of H_4SiO_4 at ~70 μM (2 ppm) (Treguer et al., 1995). However, silica concentrations show strong lateral and vertical heterogeneity in ocean basins depending on nutrient availability and uptake by diatoms in surface waters and skeleton dissolution at depth (Reynolds et al., 2006). The residence time of Si in the global oceans is ~15,000 years (Table 2) although, relative to biological uptake from surface waters, it is only ~400 years (Treguer et al., 1995), implying that Si delivered to the modern oceans is recycled ~40 times through the biological cycle before it departs into a sedimentary sink.

Bulk igneous rocks as well as co-existing mantle minerals show only limited variation in $\delta^{30}Si$ (-0.4 to -0.2) (e.g. Chakrabarti and Jacobsen, 2010; Savage et al., 2010), but chemical weathering of silicates results in lighter Si isotopes being preferentially sequestered into secondary clay minerals, which consequently display lower $\delta^{30}Si$ values (Cornelis et al., 2010; Georg et al., 2007; Opfergelt et al., 2010; Ziegler et al., 2005). The equilibrium Si isotope fractionation factor (for $\delta^{30}Si$) between kaolinite and quartz at ~27^0C is estimated at -1.6‰ (Meheut et al., 2007). Similarly, silica adsorbed on iron-oxide/hydroxide particles preferentially incorporates the lighter Si isotopes, and experimentally estimated fractionations (for $\delta^{30}Si$) range from ~1.1‰ for ferrihydrite and ~1.6‰ for goethite; this process has been proposed as a possible explanation for ^{30}Si

depletion in soils (Delstanche et al., 2009; Opfergelt et al., 2009). The suspended load of rivers typically has δ^{30}Si values similar to average igneous rocks and shales, whereas the dissolved load in rivers show higher δ^{30}Si (~ +0.8, this is about 1 to 1.2 ‰ higher than in igneous rocks), a consequence of isotope mass balance after the precipitation of ^{30}Si-depleted secondary minerals and soil formation (Ding et al., 2004; Georg et al., 2006a). Groundwaters also show enrichment in the heavier isotopes of Si (Georg et al., 2009). δ^{30}Si values for modern hydrothermal fluids from the East Pacific Rise (De la Rocha et al., 2000) are, within analytical error, identical to those of terrestrial igneous rocks; however, hydrothermal siliceous precipitates (e.g. from Mariana and Galapagos) show very light δ^{30}Si (-0.4 to -3.1) similar to sinter deposits from continental hot springs (Ding et al., 1996).

The mean δ^{30}Si of modern seawater is estimated at ~+1.1, with both spatial and depth variation in the seawater δ^{30}Si well-documented (De la Rocha et al., 2000). The higher δ^{30}Si of modern seawater compared to the continental and hydrothermal Si inputs reflects the preferential uptake of light Si isotopes by silica-secreting organisms, particularly diatoms. Si isotope fractionation factors associated with biological uptake range from ~-1.1‰ for diatoms to -3.5‰ in marine sponges (e.g. De La Rocha, 2003; De La Rocha et al., 1997; Varela et al., 2004; Beucher et al., 2008) (Table 2).

5.2. Silica cycling and Si isotopes in Precambrian oceans

Many of the same processes at work in the modern oceans were also present in the Archean and Proterozoic eons, but biological diversity, redox conditions and the relative strengths of erosional and hyodrothermal fluxes all differed from today, necessitating care in the interpretation of isotopic signatures. Silica fluxes are a corollary of the alkalinity delivered to seawater by chemical weathering of the Earth's crust. The sedimentary record of carbonate deposition reveals a pattern that is broadly similar over Earth history (Grotzinger and James, 2000), reflecting long-term commonalities in processes delivering carbon and alkalinity to seawater. Consequently, silica fluxes into Precambrian oceans were likely similar to today, if not higher, given higher hydrothermal fluxes (see below). Thus, silica must continually have left the oceans, and in the absence

of organisms producing siliceous skeletons, this occurred by means of physiochemical processes. Without known biological processes to catalyze its removal, Precambrian seawater was characterized by much higher concentrations of Si (Table 2), perhaps close to amorphous silica saturation (Siever, 1991; Siever, 1992). Some silica must have been incorporated into clays formed authigenically within sediments (e.g., Tosca et al., 2010). Much, however, left the oceans as precipitates during evaporation of seawater and is preserved primarily as early diagenetic cherts in shallow water carbonate successions (Siever, 1992). Both chert precipitation and clay formation are accompanied by Si isotopic fractionation, and so both processes should have led to enrichment of heavier Si isotopes in ambient seawater.

Banded iron formations provide another significant but more temporally restricted sink for silica. Iron formations generally contain 43-56% SiO_2 by weight (Klein, 2005) and sedimentological evidence suggests that even BIF-cherts, similar to their shallow water counterparts, form during diagenesis of precursor sediments. As most iron formations, particularly those of Archean age, reflect off-shore, commonly basinal deposition, silica precipitation was probably not forced by evaporation. Posth et al. (2008) have suggested that the alternating Si and Fe deposition in BIFs is caused by temperature fluctuations in the surface waters which slow down microbial iron mineral formation but increase abiotic silica precipitation. While seasonal fluctuations in saturation state might drive silica precipitation in shallow water, it is not clear that this mechanism would work in the open marine settings where Archean iron formations actually accumulated. Alternatively, silica may have been transported to deeper water BIFs via the 'iron shuttle' (Fischer and Knoll, 2009) by adsorption on Fe-oxide/hydroxide particles and accompanying Si isotope fractionation (c.f. Delstanche et al., 2009) leading to the progressive enrichment of heavy Si isotopes in the ambient water.

Finally, in Archean oceans, hydrothermal processes are thought to have played a particularly important role in the marine silica cycle (see below). All of the relevant sources and sinks (e.g.continental versus hydrothermal source) and processes (e.g. evaporation, adsorption onto iron minerals, precipitation, and to some extent transformation from one silica polymorph to another during diagenesis) make predictions

about the isotopic composition of ancient cherts. How might have they contributed to the observed patterns of variation?

5.3. Silica polymorphism, diagenesis, and its effect on Si isotope fractionation

Studies of deep-sea sediments indicate that during diagenesis of siliceous ooze, opal-A is transformed to opal-CT followed by chalcedony or cryptocrystalline quartz (e.g. Kastner et al., 1977). To the best of our knowledge there are no detailed studies on the effects of the above transformations on Si isotopic fractionation. The Si isotopic compositions of Phanerozoic cherts (Fig. 2) overlap with those of modern diatoms and siliceous sediments from black smokers (Robert and Chaussidon, 2006) suggesting that very little isotopic fractionation has occurred with maturation of these siliceous sediments although, closed-system experiments involving dissolution of diatom silica in seawater suggests release of fluids with δ^{30}Si lower by ~0.55‰ compared to the starting material (Demarest et al., 2009) (Table 2).

Ziegler et al. (2011) demonstrated that transformation of inorganic magadiite to quartzose chert is not accompanied by any Si isotopic fractionation; in contrast, biogenic marine opal from the Montery Formation is offset in δ^{30}Si from the cristobalitic Montery chert by 1.4‰. However, the latter offset is thought to be an imprint of a later diagenetic fluid and not necessarily due to transformation of opal-A to cristobalitic chert.

As observed in silcretes (Basile-Doelsch et al., 2005), terrestrial amorphous silica precipitates are isotopically lighter than the ambient fluid. However, the Si isotope fractionation factor between amorphous silica precipitates and water remains to be determined accurately, and may vary as a function of the precipitation mechanism as well as setting. For example, in contrast to terrestrial pedogenic and groundwater silcretes, where later-formed macro-crystalline quartz is depleted in ^{30}Si compared to the early-formed micro-crystalline quartz or the original detrital quartz, no isotopic fractionation has been observed between detrital quartz and microcrystalline quartz during marine silicification (Basile-Doelsch et al., 2005). Overall, while it may be expected that silica polymorph transformations, which involve dissolution and reprecipitation, might be

accompanied by Si isotopic fractionation, there is no strong evidence for this actually compromising isotopic measurements.

5.4. Temporal variation of δ^{30}Si in Precambrian cherts

Precambrian cherts show a large range in δ^{30}Si; this is clear from both our measurements of Late Archean and Proterozoic cherts (Fig. 2), other MC-ICPMS data from Archean samples (Abraham et al., 2011; Andre et al., 2006; Steinhoefel et al., 2009, 2010; van den Boorn et al., 2007, 2010) as well as in-situ analyses (Robert and Chaussidon, 2006; Heck et al., 2011).

We explain the temporal variation in δ^{30}Si in Precambrian cherts in light of: 1) simple mixing of silica derived from continental and hydrothermal sources, 2) mechanisms of silica precipitation and 3) equilibrium and Rayleigh-type fractionation within a single basin associated with early diagenesis.

5.4.1. Silica fluxes to the Precambrian oceans and their isotopic composition:

In the modern day, δ^{30}Si of the continental Si flux (dissolved load in rivers) is distinctly higher than that of the hydrothermal flux (hydrothermal fluids) (Table 2). It is reasonable to assume that the δ^{30}Si of hydrothermal fluids remained unchanged even in Precambrian ocean basins, even though magnitude of the hydrothermal flux to the oceans may have been different. δ^{30}Si of the continental input, however, could have varied in the past as a result of varying rates of chemical weathering or the presence of Fe^{2+} in the soil prior to the rise of oxygen.

Van den Boorn et al. (2007, 2010) categorized early Archean cherts into two types with contrasting silica sources based on petrography, trace element concentration patterns, and Si isotopic composition. Their “C-cherts,” with abundant iron hydroxides, minor carbonates and sulfides, positive Eu, La and Y anomalies, depletion in lithophile trace elements, and relatively large range in δ^{30}Si (-2.4 to +1.1), are interpreted as orthochemical primary precipitates derived from either hydrothermal fluids or mixtures of hydrothermal fluids and seawater. Their “S-cherts” contain sericite, Ti-oxides and some zircon, lack REE+Y anomalies, are enriched in lithophile elements, show a

restricted range in $\delta^{30}Si$ (+0.1 to +1.1) and are inferred to have formed by silicification of volcanogenic sediments, with the excess silica derived only from seawater.

We can reflect on this hypothesis with estimates of continental and hydrothermal fluxes to the ancient oceans based on other geochemical and isotopic proxies. Nd isotopic signatures of Precambrian BIFs reveal that the REE budget of the Archean and early Proterozoic oceans (older than ~1.9 Ga) was dominated by hydrothermal fluids circulating through mid-oceanic ridges (Jacobsen and Pimentel-Klose, 1988a, b), although locally shallow water masses may have maintained distinctly unradiogenic Nd isotopic composition, as observed in the ~2.9 Ga old Mozaan BIFs (Alexander et al., 2009). In contrast, the Nd isotopic composition of BIFs in the younger Paleoproterozoic Gunflint Formation and Neoproterozoic Urucum Formation indicate a dominantly continental source for the REEs (Jacobsen and Pimentel-Klose, 1988b). Fe/Nd ratios indicate that the predominant source of Fe in Archean and early Proterozoic BIFs and for seawater in general was hydrothermal (Jacobsen and Pimentel-Klose, 1988a, b).

REEs (Bau and Dulski, 1996; Derry and Jacobsen, 1990) support the inference from Nd isotope data and suggest that Fe and REEs derived from submarine hydrothermal systems co-precipitated from seawater as Fe-oxy-hydroxides in precursor sediments to BIFs. Seawater Sr isotopic composition shows a change from mantle-like $^{87}Sr/^{86}Sr$ before 2.5 Ga towards increasingly radiogenic $^{87}Sr/^{86}Sr$ afterward (Shields and Veizer, 2002). The shift towards more radiogenic Sr and less radiogenic Nd near the Archean-Proterozoic boundary is thought to reflect a change from a ‘‘mantle’’-buffered to a ‘‘continent’’-buffered global seawater composition around this time and is likely to result from a combination of decreasing heat flux from the mantle and intensified formation of continental crust. However, Si isotopic variability in Precambrian cherts do not show any dramatic change from low $\delta^{30}Si$, akin to hydrothermal sources, to higher values (similar to the dissolved load in rivers) at around 2.5 Ga (Fig 2). One possibility is that estimating continental and hydrothermal fluxes based on REE concentration patterns or Nd and Sr isotopes might not be directly applicable to Si. In the modern oceans, while REE concentrations increase with depth, they are not correlated with Si concentrations, suggesting a decoupling between the REE cycle and the Si cycle. REE concentrations continue to increase with depth even after Si and PO_4^{3-} have reached their deep-water

maxima (Piepgras and Jacobsen, 1992). However, this decoupling could be due to the effect of organisms on Si concentration and might not be applicable to the Precambrian. Si concentrations, however, co-vary with the Nd isotopic composition of Pacific bottom water and follow a mixing trend (Piepgras and Jacobsen, 1988).

In contrast to REE and Nd isotope studies, Ge/Si measurements of the silica rich layers in BIF from the 2.5 Ga old Dales Gorge Member of the Hamersley Group suggest that silica in these BIFs was derived by weathering of continental land mass, whereas the iron has a hydrothermal origin (Hamade et al., 2003). However, this hypothesis requires that chemical precipitation of silica does not fractionate Ge from Si and that the Ge/Si ratio of continental and hydrothermal sources has remained constant over time. This does not appear to be the case (Anders et al., 2003; Fischer and Knoll, 2009; Hammond et al., 2000; Pokrovsky et al., 2006). In addition, it is not clear how the Ge/Si ratio is affected by diagenesis (Hamade et al., 2003).

Clearly, temporal variations of δ^{30}Si in cherts cannot be explained solely by simple mixing of isotopically distinct continental and hydrothermal sources, unlike seawater Nd and Sr isotope variations over time. Additional mechanisms need to be invoked; these are discussed below.

5.4.2. Mechanism of silica precipitation:

Cherts associated with iron formations tend to have lower δ^{30}Si values than non-BIF peritidal cherts, even in the same basin (Fig. 2, 3). For example, within the Late Archean Transvaal basin, peritidal cherts tend to be at least 1‰ higher in δ^{30}Si than BIF cherts deposited at depth. This is consistent with the hypothesis of hydrothermal versus continental origins of silica (Andre et al., 2006; Steinhoefel et al., 2009; Steinhoefel et al., 2010; Heck et al., 2011) We postulate that δ^{30}Si in Precambrian cherts not only reflects the source of silica but also the depositional conditions and the mechanism by which silica was precipitated.

The relatively low Si-isotopic values of cherts in iron formation could reflect deposition by adsorption onto Fe-oxide/hydroxide particles consistent with observations from laboratory experiments (Delstanche et al., 2009. Silica adsorption onto iron oxides/hydroxides would also have occurred in soils following the initial oxygenation of

463 the atmosphere and surface ocean 2.3-2.45 Ga (Holland, 2006), resulting in a higher δ^{30}Si
464 of continental silica entering the oceans.
465 Thus, in concert, changing hydrothermal fluxes into the oceans and Earth's
466 evolving redox state provide a reasonable first order explanation for the observed
467 increase in chert δ^{30}Si values from early Archean through mid-Proterozoic time. These
468 factors may also explain the observed decease in mean δ^{30}Si values for Neoproterozoic
469 cherts. This explanation is consistent with Sr isotopic studies which suggest reinvigorated
470 hydrothermal influence on seawater in association with Neoproterozoic continental
471 breakup (e.g., Asmerom et al., 1991; Halverson et al., 2007), and Fe speciation analyses
472 which indicate a return to ferruginous subsurface water masses at this time (Johnston et
473 al., 2010), if not earlier (Planavsky et al., 2011).
474 Against this backdrop, the remarkably low δ^{30}Si of the oolitic iron formation of
475 the Paleoproterozoic Frere Formation (-2.68), Western Australia, and basinal cherts
476 associated with the possibly coeval Duck Creek Formation (-4.29), Western Australia,
477 deserve special mention. Although such low δ^{30}Si values are rare in our dataset, similarly
478 values have been reported in BIFs from Isua and the Transvaal craton and explained as
479 hydrothermally derived Si that has been further fractionated by adsorption on to Fe-
480 hydroxide as well as later crystallization (Heck et al., 2011). Such an explanation may
481 well apply to our late Paleoproterozoic samples, consistent with the hypothesis that this
482 resurgence of iron formation after several hundred years' absence reflects a superplume
483 (Condie, 2004).
484
485 *5.4.3. Si isotopic variation in peritidal cherts from individual basins*
486 Si-isotopic values within the late Archean Transvaal basin vary by nearly 3‰,
487 explainable, at least in part, by differences between peritidal and basin BIF cherts. The 25
488 chert samples measured from the ~750-800 Ma old Akademikerbreen Group,
489 Spitsbergen, and its correlatives in Nordaustlandet and East Greenland, show a
490 comparable range of δ^{30}Si values from -1.78 to +1.26. For the latter sample set, however,
491 another explanation is required to explain the observed variation, as all come from early
492 diagenetic cherts within peritidal carbonate facies.

493 Variation in $\delta^{30}Si$ in the Spitsbergen cherts can be explained by fractionation
494 during precipitation from silica-saturated porewaters. The $\delta^{30}Si$ evolution of the
495 precipitates and the fluid can be modeled for both a closed system (i.e. precipitate is in
496 equilibrium with the ambient fluid) and an open system (Rayleigh fractionation, i.e.
497 precipitate is removed from the system) using standard equations (c.f. Criss, 1999) and
498 are shown in Figure 4. The Si isotope fractionation factor between silica saturated fluids
499 and silica precipitating from them is not well constrained although it is known that
500 chemical precipitates preferentially incorporate the lighter Si isotopes (e.g. Basile-
501 Doelsch et al., 2005). In this model, the fractionation between the fluid (silica saturated
502 porewater) and the precipitate (cherts), which increases with decreasing temperature, is
503 such that in Case 1 the precipitate is 2.0 ‰ lower than the fluid and in Case 2 it is 3.0 ‰
504 lower. The initial $\delta^{30}Si$ of the fluid is assumed to be 0.8 ‰, similar to the $\delta^{30}Si$ of modern
505 dissolved load in rivers. Although the absolute values of the fractionation factors are
506 arbitrarily chosen, they are consistent with fractionations in other natural systems (Table
507 2). Using the above parameters, the entire range in $\delta^{30}Si$ in the Spitsbergen cherts (~3‰)
508 can be explained by a Rayleigh-type isotope fractionation with f ranging from 1 to 0.2.
509 Fractionations are much smaller for the equilibrium/closed-system scenario. The $\delta^{30}Si$
510 range in cherts at any instant of time could be explained by a similar mechanism. Thus
511 we interpret the large range of values in the peritidal cherts as being due to fractional
512 crystallization of the silicifying fluid that replaced the initial limestones with cherts.
513 We also consider the effect of early-diagenesis on the Si isotopic composition of
514 amorphous siliceous precipitates as some of our samples show indications of later
515 diagenetic modification. As discussed in Section 5.2, transformation from amorphous
516 opal-A to micro-crystalline quartz involves dissolution and reprecipitation which is
517 expected to be accompanied by Si isotope fractionation, although there is no convincing
518 evidence thus far for such an effect. Nevertheless, it has been observed that dissolution of
519 biogenic opal in seawater releases light isotopes of Si ($\delta^{30}Si$ light by 0.5 ‰) (Demarest et
520 al., 2009) while precipitates also favor the light Si isotopes (e.g. Basile-Doelsch et al.,
521 2005). Hence, the net isotope fractionation between silica saturated porewaters and chert
522 can be considered as an additive effect of precipitation and continued dissolution and
523 could contribute to the large $\delta^{30}Si$ range in cherts at any instant of time.

The high Si content in cherts makes Si isotopic composition of cherts less susceptible to pervasive post-depositional changes (e.g. Heck et al., 2011, Marin-Carbonne et al., 2011). This is consistent with the large variations observed in peritidal cherts; any pervasive late-stage modification would have resulted in a more uniform Si isotopic composition in these samples. This conclusion is consistent with recent in-situ measurements of Si isotopes in Archean BIFs (Heck et al., 2011).

5.5. Toward understanding the temporal variation in the Si isotopic composition of Precambrian seawater

The isotopic composition of ancient seawater can be reconstructed from analyses of chemical precipitates derived from seawater (e.g. Shields and Veizer, 2002). However, post-depositional alteration often obliterates the pristine seawater isotopic signature as observed in Sr, C and O isotopic studies of carbonates; the extent to which post-depositional overprinting occurs depends on the concentration of the element in the rock versus the diagenetic fluid (c.f. Jacobsen and Kaufman, 1999). It has been argued that the low permeability of cherts make them less prone to late-dissolution/reprecipitation events compared to carbonates and low water/rock ratios during metamorphic heating does not result in perturbation of $\delta^{18}O$ in cherts (c.f. Knauth, 2005). $\delta^{18}O$ in Precambrian cherts show a gradual change from ^{18}O-depleted values in the Archean to more enriched values in the Neoproterozoic. This is been interpreted to reflect warm ocean waters (55-85 ^{0}C) in the Archean to cooler temperatures with time (Knauth, 2005 and references therein, Marin et al., 2010). Based on an observed positive correlation between Si and O isotopic values in Precambrian cherts, Robert and Chaussidon (2006) interpreted secular variations in Si-isotopic composition of seawater in terms of a single reservoir with a single silica source from weathering and two sinks, sedimentary rocks and hydrothermal alteration of the crust, respectively. Given knowledge of the isotope fractionation during hydrothermal silicification (admittedly poorly constrained) and measurements of the isotopic composition of the sedimentary sink, this system can be solved for the fraction of silica that departs in the sedimentary sink; if correct, this framework provides the logic for a proxy of seawater temperature (due to the temperature dependence of amorphous

555 silica solubility) (Robert and Chaussidon, 2006) similar to oxygen isotopes. However, it
556 is difficult to characterize the sedimentary Si flux with any single δ^{30}Si value as discussed
557 before, complicating the hypothesis of Robert and Chaussidon (2006). While it is
558 possible that O isotopes in Archean cherts reflect warm temperatures, the temperatures
559 are warm because the ambient waters were hydrothermal, not seawater (e.g., Blake et al.,
560 2010; Pope et al., 2012). To the extent that this is the case, Si and O isotopes might
561 covary in Archean cherts not because they both record seawater T but because both
562 reflect declining hydrothermal input through time.

563 The Si isotopic composition of seawater at any given moment in the Precambrian
564 was likely a function of the Si isotopic composition of continental and hydrothermal
565 inputs and outputs (peritidal chert precipitation and BIF formation), their relative fluxes,
566 and the isotopic fractionation factors related to precipitation of silica from seawater or
567 porewater ($\Delta_{SW-chert}$) and/or adsorption of silica onto Fe-hydroxide particles during BIF
568 formation (Δ_{SW-BIF}). Given the long residence time of Si relative to mixing times of the
569 ocean (Table 2), it is likely that Si in Precambrian cherts was derived from seawater with
570 relatively uniform Si isotope composition. Hence, δ^{30}Si variations in cherts over time
571 may indirectly reflect the temporal variation of δ^{30}Si of the seawater. As discussed above,
572 δ^{30}Si of chemical precipitates (e.g. cherts) tend to be lower than that of the ambient
573 solution (e.g. seawater or porewater). In addition, the fractionations associated with
574 various Si sources and sinks may have changed or been differentially expressed
575 throughout Proterozoic time (e.g. during times of banded iron formation deposition or
576 enhanced authigenic clay formation). In the absence of well-constrained fractionation
577 factors, we present a qualitative analysis of factors than can cause variation in the
578 seawater δ^{30}Si.

579 Let us first consider a simple case, where the continental and hydrothermal Si
580 fluxes to the ocean, their isotopic compositions as well as the isotopic fractionation
581 factors during chert and BIF formation remain constant over Earth history. Even with a
582 significant fractionation during precipitation, the isotopic composition of cherts would
583 show no variation with time. However, if the relative contributions of continental and
584 hydrothermal fluxes of silica to the oceans varied over time as suggested by Nd isotopes

585 (e.g. Jacobsen and Pimentel-Klose, 1988a,b), the $\delta^{30}Si$ variation in cherts from 3.8 Ga to
586 1.5 Ga may reflect a gradual change from hydrothermal to continental silica sources. If
587 correct, this would suggest an important change in the locus of silicate weathering during
588 Proterozoic time.

589 Additionally, the silicon isotopic composition of the continental flux could also
590 have varied with time. Increased clay genesis during soil formation, including
591 interactions of Si with ferric oxides after the rise of atmospheric oxygen, would result in
592 preferential removal of light Si on particles, and an increase in the $\delta^{30}Si$ of the dissolved
593 load in rivers ultimately delivered to the oceans. Extent of silica depletion as well as
594 wetter versus drier climates can also alter soil $\delta^{30}Si$ (Bern et al., 2010). These processes
595 could also explain the high $\delta^{30}Si$ in Mid-Proterozoic cherts, which is a prominent feature
596 in both our dataset and that of Robert and Chaussidon (2006).

597 The reversal in the above trend towards lower $\delta^{30}Si$ since 1.5 Ga is harder to
598 explain. One possibility is an increased flux of light hydrothermal source-derived Si into
599 the oceans associated with Neoproterozoic breakup of Rodinia (e.g. Dalziel, 1997; Evans,
600 2009; Pisarevsky et al., 2003). However, this does not explain why values begin to
601 decline as early as 1.2 Ga. Moreover, other isotopic proxies of paleo-seawater
602 composition like Nd, Sr isotopes do not show any evidence of an increased hydrothermal
603 flux of Si (low $\delta^{30}Si$) beginning 1.5 Ga ago. Alternatively, the disappearance of BIFs
604 (very low $\delta^{30}Si$) at ~1.8 Ga would leave the ambient seawater relatively less enriched in
605 the heavier Si isotopes and this would be reflected in lower $\delta^{30}Si$ in peritidal cherts
606 precipitating from this seawater. The timing of the general disappearance of iron
607 formation deposits from the sedimentary record, however, occurs several hundred million
608 years too early to easily satisfactorily explain this trend. Moreover, continued
609 precipitation of cherts (low $\delta^{30}Si$) would result in progressively higher $\delta^{30}Si$ in younger
610 cherts, which is in contrast to the observed trend.

611 The decreasing $\delta^{30}Si$ trend in cherts since 1.5 Ga ago continues into the
612 Phanerozoic, even though the marine silica cycle changed drastically in the Phanerozoic
613 due to evolution of silica secreting organisms, which preferentially take up the lighter
614 isotopes of Si. In the presence of silica secreting organisms, the seawater $\delta^{30}Si$ and hence

that of cherts precipitating from it should have been higher in the Phanerozoic than what is observed (Fig 2). This suggests that abiotic mechanisms, similar to the ones discussed above, may be the dominant drivers of the Si isotopic composition of the seawater over time.

6. CONCLUSIONS

We have presented the first high-precision MC-ICPMS measurements of the Si isotopic composition of Proterozoic cherts. These samples, collected from a wide range of sedimentary settings from different parts of the world, show large variations in δ^{30}Si, from +2.85 to -4.29. These trends reflect, in part, variable contributions between isotopically distinct hydrothermal and continental sources of silica to seawater. Additionally, δ^{30}Si variability reflects clear paleoenvironmental differences in chert petrogenesis, including the redox profile of ambient ocean basins. In combination with other available MC-ICPMS measurements of Precambrian cherts, our data indicate that peritidal cherts, formed by early diagenetic replacement of carbonates, show relatively high δ^{30}Si compared to basinal cherts associated with BIFs. We suggest that such contrasting δ^{30}Si in cherts reflect the mechanisms of silica precipitation. Shallow water cherts precipitate out of silica-saturated porewaters, primarily driven by evaporation, whereas silica in basinal cherts associated with BIFs was transported to deeper waters by adsorption onto Fe-hydroxide particles. Laboratory experiments showing that silica adsorption onto Fe-hydroxide particles preferentially deposits lighter Si isotopes is consistent with the relatively low δ^{30}Si observed in BIFs. Additionally, the lower δ^{30}Si in BIFs could also reflect Si being primarily derived from hydrothermal sources. The large variation in δ^{30}Si of peritidal cherts from a single basin can be explained by Rayleigh-type fractionation during precipitation from silica-saturated porewaters. There is no evidence thus far to suggest that silica polymorph transformation during chert formation results in significant Si isotope fractionation. Post-depositional dissolution and reprecipitation of silica could have contributed to the large range in δ^{30}Si in a single basin but high silica in cherts makes δ^{30}Si values less susceptible to pervasive post-depositional changes.

Despite differential fractionations due to paleoenvironmental differences and precipitation processes, the global dataset shows a broad pattern of temporal variability. $\delta^{30}Si$ increase monotonically from 3.8 Ga to 1.5 Ga, attributed to varying continental versus hydrothermal silica fluxes to the oceans as well as isotopic fractionation related to precipitation of cherts and BIFs. A Mesoproterozoic $\delta^{30}Si$ maxima observed in 1.5 Ga old peritidal cherts may reflect an increase in Si isotope fractionation during soil forming processes (possibly related to higher atmospheric oxygen concentrations and more ferric iron in soil horizons) which increased the $\delta^{30}Si$ of the dissolved load of rivers and consequently seawater. The causes behind decreasing $\delta^{30}Si$ in cherts from 1.5 Ga onward remain unclear. However this trend continues into Phanerozoic time, suggesting an underlying similarity in the dominant factors controlling the silicon isotopic composition of seawater through the later Proterozoic and Phanerozoic eons.

*Acknowledgements:*This work was supported by NASA Cosmochemistry Program grants #NNX07AF86G #NNX10AI43G to SBJ. RC thanks the Origins of Life Initiative at Harvard University for his post-doctoral support. AHK and WWF thank the Agouron Institute and AHK thanks the NASA Astrobiology Institute for support. We thank Dr. Philipp Heck and two other anonymous reviewers and the Associate Editor Dr. Clark Johnson for their comments and suggestions.

REFERENCES

Abraham, K., Hofmann, A., Foley, S.F., Cardinal, D., Harris, C., Barth, M.G., and Andre, L. (2011) Coupled silicon-oxygen isotope fractionation traces Archaean silicification. *Earth Planet. Sci. Lett.* **301**, 222-230.

Alexander, B.W., Bau, M., and Andersson, P. (2009) Neodymium isotopes in Archean seawater and implications for the marine Nd cycle in Earth's early oceans. *Earth Planet. Sci. Lett.* **283**, 144-155.

Allison, C. W., and Awramik, S.M. (1989) Organic-walled microfossils from earliest Cambrian or latest Proterozoic Tinder Group rocks, Northwest Canada. *Precamb. Res*. **43**, 253-294.

676 Anders, A.M., Sletten, R.S., Derry, L.A., and Hallet, B. (2003) Germanium/silicon ratios
677 in the Copper River Basin, Alaska: Weathering and partitioning in periglacial
678 versus glacial environments. *J. Geophys. Res.* **108**, 6005, doi:
679 10.1029/2003JF000026.
680 Andre, L., Cardinal, D., Alleman, L.Y., and Moorbath, S., 2006, Silicon isotopes in 3.8
681 Ga West Greenland rocks as clues to the Eoarchaean supracrustal Si cycle. *Earth*
682 *Planet. Sci. Lett.* **245**, 162-173.
683 Asmerom, Y., Jacobsen, S.B., Knoll, A.H., Butterfield, N.J., and Swett, K., 1991,
684 Strontium Isotopic Variations of Neoproterozoic Seawater - Implications for
685 Crustal Evolution. *Geochim. Cosmochim. Acta* **55**, 2883-2894.
686 Barghoorn, E.S., and Tyler, S.A. (1965) Microorganisms from the Gunflint Chert.
687 *Science* **147**, 563-577.
688 Basile-Doelsch, I., Meunier, J.D., and Parron, C. (2005) Another continental pool in the
689 terrestrial silicon cycle. *Nature* **433**, 399-402.
690 Bau, M., and Dulski, P. (1996), Distribution of yttrium and rare-earth elements in the
691 Penge and Kuruman iron-formations, Transvaal Supergroup, South Africa.
692 *Precamb. Res.* **79**, 37-55.
693 Bern, C. R., Brzezinski, M. A., Beucher, C., Ziegler, K., and Chadwick, O. A. (2010)
694 Weathering, dust, and biocycling effects on soil silicon isotope ratios. *Geochim.*
695 *Cosmochim. Acta* **74**, 876-889.Beucher, C. P., Brzezinski, M. A., and Jones, J. L.,
696 (2008), Sources and biological fractionation of Silicon isotopes in the Eastern
697 Equatorial Pacific. *Geochim. Cosmochim. Acta* **72**, 3063-3073.
698 Blake, R.E., Chang, S.J., and Lepland, A. (2010) Phopshate oxygen isotope evidence for
699 a temperate and biologically active Archean ocean. *Nature* **464**, 1029-1232.
700 Brotton, S. J., Shapiro, R., van der Laan, G., et al. (2007) Valence state fossils in
701 Proterozoic stromatolites by L-edge X-ray absorption spectroscopy. *Jour.*
702 *Geophys. Res. Biogeosc.* **112**, G03004 DOI: 10.1029/2006JG000185.
703 Chakrabarti, R., and Jacobsen, S.B. (2010) Silicon isotopes in the inner Solar System:
704 Implications for core formation, solar nebular processes and partial melting.
705 *Geochim. Cosmochim. Acta* **74**, 6921-6933.

706 Condie, K.C. (2004) Supercontinents and superplume events: distinguishing signals in
707 the geologic record. *Physics Earth Planet. Int.* **146**, 319-332.
708 Cornelis, J.T., Delvaux, B., Cardinal, D., Andre, L., Ranger, J., and Opfergelt, S. (2010)
709 Tracing mechanisms controlling the release of dissolved silicon in forest soil
710 solutions using Si isotopes and Ge/Si ratios. *Geochim. Cosmochim. Acta*. **74**,
711 3913-3924.
712 Criss, R. E. (1999) *Principles of Stable Isotope Distribution*. New York, Oxford
713 University Press.
714 Dalziel, I. W. D. (1997) Neoproterozoic-Paleozoic geography and tectonics: Review,
715 hypothesis, environmental speculation. *Geological Society of America Bulletin*
716 **109**, 16-42.
717 Dawes, P.R. (1997) The Proterozoic Thule Supergroup, Greenland and Canada: history,
718 lithostratigraphy and development. *Greenland Geological Survey Bulletin* **174**, 1-
719 150.
720 De La Rocha, C.L. (2003) Silicon isotope fractionation by marine sponges and the
721 reconstruction of the silicon isotope composition of ancient deep water. *Geology*
722 **31**, 423-426.
723 De La Rocha, C.L., Brzezinski, M.A., and DeNiro, M.J. (1997) Fractionation of silicon
724 isotopes by marine diatoms during biogenic silica formation. *Geochim.*
725 *Cosmochim. Acta* **61**, 5051-5056.
726 De la Rocha, C.L., Brzezinski, M.A., and DeNiro, M.J. (2000) A first look at the
727 distribution of the stable isotopes of silicon in natural waters. *Geochim.*
728 *Cosmochim. Acta* **64**, 2467-2477.
729 Delstanche, S., Opfergelt, S., Cardinal, D., Elsass, F., Andre, L., and Delvaux, B. (2009)
730 Silicon isotopic fractionation during adsorption of aqueous monosilicic acid onto
731 iron oxide. *Geochim. Cosmochim. Acta* **73**, 923-934.
732 Demarest, M. S., Brzezinski, M. A., and Beucher, C. P. (2009) Fractionation of silicon
733 isotopes during biogenic silica dissolution. *Geochim. Cosmochim. Acta* **73**, 5572-
734 5583.

735 Derry, L.A., and Jacobsen, S.B. (1990) The Chemical Evolution of Precambrian Seawater
736 - Evidence from Rees in Banded Iron Formations. *Geochim. Cosmochim. Acta* **54**,
737 2965-2977.
738 Ding, T., Jiamg, S., Wan, D., Li, Y., Li, J., Song, H., Liu, Z., and Yao, X. (1996) *Silicon*
739 *isotope geochemistry*. Beijing, China, Geological Publishing House.
740 Ding, T., Wan, D., Wang, C., and Zhang, F. (2004) Silicon isotope compositions of
741 dissolved silicon and suspended matter in the Yangtze River, China. *Geochim.*
742 *Cosmochim. Acta* **68**, 205-216.
743 Evans, D.A.D. (2009). The palaeomagnetically viable, long-lived and all-inclusive
744 Rodinia supercontinent reconstruction. In *Ancient Orogens and Modern*
745 *Analogues* (eds. J. B. Murphy, J. D. Keppie and A. Hynes), Geological Society of
746 London Special Publication 327, pp 371-404.
747 Fischer, W.W., and Knoll, A.H. (2009) An iron shuttle for deepwater silica in Late
748 Archean and early Paleoproterozoic iron formation. *Geological Society of*
749 *America Bulletin* **121**, 222-235.
750 Georg, R.B., Reynolds, B.C., Frank, M., and Halliday, A.N. (2006a) Mechanisms
751 controlling the silicon isotopic compositions of river waters. *Earth Planet. Sci.*
752 *Lett.* **249**, 290-306.
753 Georg, R.B., Reynolds, B.C., Frank, M., and Halliday, A.N. (2006b) New sample
754 preparation techniques for the determination of Si isotopic compositions using
755 MC-ICPMS. *Chem.Geol.* **235**, 95-104.
756 Georg, R.B., Reynolds, B.C., West, A.J., Burton, K.W., and Halliday, A.N. (2007)
757 Silicon isotope variations accompanying basalt weathering in Iceland. *Earth*
758 *Planet. Sci. Lett.* **261**, 476-490.
759 Georg, R.B., West, A.J., Basu, A.R., and Halliday, A.N. (2009) Silicon fluxes and isotope
760 composition of direct groundwater discharge into the Bay of Bengal and the effect
761 on the global ocean silicon isotope budget. *Earth Planet. Sci. Lett.* **283**, 67-74.
762 Green, J.W., Knoll, A.H., and Swett, K. (1989) Microfossils from silicified stromatolitic
763 carbonates of the Upper Proterozoic Limestone-Dolomite 'Series', central East
764 Greenland. *Geol. Mag.* **126**, 567-585.

765 Grotzinger, J.P., and James, N.P. (2000) Precambrian carbonates: evolution of
766 understanding, In *Carbonate Sedimentation and Diagenesis in the Evolving*
767 *Precambrian World* (eds. J. P. Grotzinger and N. P. James), SEPM Special
768 Publication 67, Tulsa, OK, pp. 3-20.
769 Halverson, G.P., Dudas, F.O., Maloof, A.C., and Bowring, S.A. (2007) Evolution of the
770 $^{87}Sr/^{86}Sr$ composition of Neoproterozoic seawater. *Palaeogeography*
771 *Palaeoclimatology Palaeoecology* **256**, 103-129.
772 Hamade, T., Konhauser, K.O., Raiswell, R., Goldsmith, S., and Morris, R.C. (2003)
773 Using Ge/Si ratios to decouple iron and silica fluxes in Precambrian banded iron
774 formations. *Geology* **31**, 35-38.
775 Hammond, D.E., McManus, J., Berelson, W.M., Meredith, C., Klinkhammer, G.P., and
776 Coale, K.H. (2000) Diagenetic fractionation of Ge and Si in reducing sediments:
777 The missing Ge sink and a possible mechanism to cause glacial/interglacial
778 variations in oceanic Ge/Si. *Geochim. Cosmochim. Acta* **64**, 2453-2465.
779 Heck, P. R., Huberty, J. M., Kita, N. T., Ushikubo, T., Kozdon, R., Valley, J. W. (2011)
780 SIMS analyses of silicon and oxygen isotope ratios for quartz from Archean and
781 Paleoproterozoic banded iron formations. *Geochim. Cosmochim. Acta* **75**, 5879-
782 5894.
783 Holland, H.D. (2006) The oxygenation of the atmosphere and oceans. *Phil. Trans. Royal*
784 *Soc. B* **361**, 903-915.
785 Jacobsen, S.B., and Pimentel-Klose, M.R. (1988a) A Nd Isotopic Study of the Hamersley
786 and Michipicoten Banded Iron Formations - the Source of REE and Fe in Archean
787 Oceans. *Earth Planet. Sci. Lett.* **87**, 29-44.
788 Jacobsen, S.B., and Pimentel-Klose, M.R. (1988b) Nd Isotopic variations in Precambrian
789 Banded Iron Formations. *Geophys. Res. Lett.* **15**, 393-396.
790 Jacobsen, S.B., and Kaufman, A. J. (1999) The Sr, C and O isotopic evolution of
791 Neoproterozoic seawater. *Chem. Geol.* **161**, 37-57.
792 Johnston, D.T., Poulton, S.W., Dehler, C., Porter, S., Husson, J., Canfield, D.E., and
793 Knoll, A.H. (2010) An emerging picture of Neoproterozoic ocean chemistry:
794 Insights from the Chuar Group, Grand Canyon, USA. *Earth Planet. Sci. Lett.* **290**,
795 64-73.

796 Kah, L.C., and Knoll, A.H. (1996) Microbenthic distribution of proterozoic tidal flats:
797 Environmental and taphonomic considerations. *Geology* **24**, 79-82.
798 Kastner, M., Keene, J. B., Gieskes, J. M. (1977) Diagenesis of siliceous oozes - I.
799 Chemical controls on the rate of opal-A to opal-CT transformation - an
800 experimental study. *Geochim. Cosmochim. Acta* **41**, 1041-1059.
801 Klein, C. (2005) Some Precambrian banded iron-formations (BIFs) from around the
802 world: Their age, geologic setting, mineralogy, metamorphism, geochemistry, and
803 origin. *American Mineralogist* **90**, 1473-1499.
804 Knauth, L. P. (2005) Temperature and salinity history of the Precambrian ocean:
805 implications for the course of microbial evolution. *Paleogeog. Paleoclim.*
806 *Paleoecol.* **219**, 53-69.
807 Knoll, A. (1985) Exceptional preservation of photosynthetic organisms in silicifed
808 carbonates and silicified peats. *Phil. Trans. Royal Soc. London* **311**, 11-122.
809 Knoll, A.H. (1984) Microbiotas of the late Precambrian Hunnberg Formation,
810 Nordaustlandet, Svalbard. *Journal of Paleontology* **58**, 131-162.
811 Knoll, A.H., and Beukes, N.J. (2009) Introduction: Initial investigations of a Neoarchean
812 shelf margin-basin transition (Transvaal Supergroup, South Africa). *Precamb.*
813 *Res.* **169**, 1-14.
814 Knoll, A.H., and Swett, K. (1990) Carbonate Deposition during the Late Proterozoic Era
815 - an Example from Spitsbergen. *American Journal of Science* **290A**, 104-132.
816 Knoll, A.H., Swett, K., and Burkhardt, E. (1989) Paleoenvironmental Distribution of
817 Microfossils and Stromatolites in the Upper Proterozoic Backlundtoppen
818 Formation, Spitsbergen. *Journal of Paleontology* **63**, 129-145.
819 Knoll, A.H., Swett, K., and Mark, J. (1991) Paleobiology of a Neoproterozoic Tidal Flat
820 Lagoonal Complex - the Draken Conglomerate Formation, Spitsbergen. *Journal*
821 *of Paleontology* **65**, 531-570.
822 Macdonald, F.A., Cohen, P.A., Dudas, F.O., and Schrag, D.P. (2010) Early
823 Neoproterozoic scale microfossils in the Lower Tindir Group of Alaska and the
824 Yukon Territory. *Geology* **38**, 143-146.
825 Macdonald, F.A., Smith, E. F., Strauss, J. V., Cox, G. M., Halverson, G. P. & Roots, C.
826 F. (2011). Neoproterozoic and early Paleozoic correlations in the western Ogilvie

827 Mountains, Yukon. *In: MacFarlane, K. E., Weston, L. H. & Blackburn, L. R.*
828 *(eds) Yukon Exploration and Geology 2010. Yukon Geological Survey,*
829 *Whitehorse*, 161–182.
830 Maliva, R.G., Knoll, A.H., and Siever, R. (1989) Secular change in chert distribution: a
831 reflection of evolving biological participation in the silica cycle. *Palaios* **4**, 519-
832 532.
833 Maliva, R.G., Knoll, A.H., and Simonson, B.M. (2005) Secular change in the
834 Precambrian silica cycle: Insights from chert petrology. *Geological Society of*
835 *America Bulletin* **117**, 835-845.
836 Marin, J., Chaussidon, M., and Robert, F. (2010) Microscale oxygen isotope variations in
837 1.9 Ga Gunflint cherts: Assessments of diagenesis effects and implications for
838 oceanic paleotemperature reconstructions. *Geochim. Cosmochim. Acta* **74**, 116-
839 130.
840 Marin-Carbonne, J., Chaussidon, M., Boiron, Marie-Christine and Robert, F. (2011) A
841 combined in situ oxygen, silicon isotopic and fluid inclusion study of a chert
842 sample from Onverwacht Group (3.35 Ga, South Africa): New constraints on
843 fluid circulation. *Chem. Geol.* **286**, 59-71.
844 Meheut, M., Lazzeri, M., Balan, E., and Mauri, F. (2007) Equilibrium isotopic
845 fractionation in the kaolinite, quartz, water system: Prediction from first-
846 principles density-functional theory. *Geochim. Cosmochim. Acta* **71**, 3170-3181.
847 Opfergelt, S., Cardinal, D., Andre, L., Delvigne, C., Bremond, L., and Delvaux, B. (2010)
848 Variations of δ^{30}Si and Ge/Si with weathering and biogenic input in tropical
849 basaltic ash soils under monoculture. *Geochim. Cosmochim. Acta* **74**, 225-240.
850 Opfergelt, S., de Bournonville, G., Cardinal, D., Andre, L., Delstanche, S., and Delvaux,
851 B. (2009) Impact of soil weathering degree on silicon isotopic fractionation
852 during adsorption onto iron oxides in basaltic ash soils, Cameroon. *Geochim.*
853 *Cosmochim. Acta* **73**, 7226-7240.
854 Piepgras, D.J., and Jacobsen, S.B. (1988) The Isotopic Composition of Neodymium in
855 the North Pacific. *Geochim. Cosmochim. Acta* **52**, 1373-1381.

856 Piepgras, D.J., and Jacobsen, S.B. (1992) The Behavior of Rare-Earth Elements in
857 Seawater - Precise Determination of Variations in the North Pacific Water
858 Column. *Geochim. Cosmochim. Acta* **56**, 1851-1862.
859 Pisarevsky S.A., Wingate M.T.D., Powell C. McA., Johnson S. & Evans D.A.D. (2003)
860 Models of Rodinia assembly and fragmentation. In *Proterozoic East Gondwana:*
861 *Super Continent Assembly and Break-up* (eds. M. Yoshida, B. Windley & S.
862 Dasgupta), Geological Society of London Special Publication, 206, pp 35-55.
863 Planavsky, N.J., McGoldrick, P., Scott, C.T., Li, C., Reinhard, C.T., Kelly, A.E., Chu, X.,
864 Bekker, A., Love, G.D., and Lyons, T.W. (2011) Widespread iron-rich
865 conditions in the mid-Proterozoic ocean. *Nature*, doi:10.1038/nature10327.
866 Pokrovsky, O.S., Pokrovski, G.S., Schott, J., and Galy, A. (2006) Experimental study of
867 germanium adsorption on goethite and germanium co-precipitation with iron
868 hydroxide: X-ray absorption fine structure and macroscopic characterization.
869 *Geochim. Cosmochim. Acta* **70**, 3325-3341.
870 Pope, E.C., Bird, D.K., and Rosing, M.T. (2012) Isotope composition and volume of
871 Earth's early oceans. *Proc. Nat. Acad. Sci, USA* **109**, 4371-4376.
872 Posth, N.R., Hegler, F., Konhauser, K.O., and Kappler, A. (2008) Alternating Si and Fe
873 deposition caused by temperature fluctuations in Precambrian oceans. *Nature*
874 *Geoscience* **1**, 703-708.
875 Reynolds, B.C., Aggarwal, J., Andre, L., Baxter, D., Beucher, C., Brzezinski, M.A.,
876 Engstrom, E., Georg, R.B., Land, M., Leng, M.J., Opfergelt, S., Rodushkin, I.,
877 Sloane, H.J., van den Boorn, S.H.J.M., Vroon, P.Z., and Cardinal, D. (2007) An
878 inter-laboratory comparison of Si isotope reference materials. *J. Anal. Atom.*
879 *Spectrom.* **22**, 561-568.
880 Reynolds, B.C., Jaccard, S.L., and Haliday, A.N. (2006) Abrupt cessation of north pacific
881 upwelling with Northern Hemisphere Glaciation recorded by silicon isotopes.
882 *Geochim. Cosmochim. Acta* **70**, A530 (Abstr.).
883 Robert, F., and Chaussidon, M. (2006) A palaeotemperature curve for the Precambrian
884 oceans based on silicon isotopes in cherts. *Nature* **443**, 969-972.

885 Savage, P.S., Georg, R.B., Armytage, R.M.G., Williams, H.M., and Halliday, A.N.
886 (2010) Silicon isotope homogeneity in the mantle. *Earth Planet. Sci. Lett.* **295**,
887 139-146.
888 Sergeev, V.N., Knoll, A.H., and Grotzinger, J.P. (1995) Paleobiology of the
889 Mesoproterozoic Billyakh Group, Anabar uplift, Northern Siberia. *Paleontogical*
890 *Society Mem.* **39**, 1-37.
891 Sergeev, V.N., Knoll, A.H., and Petrov, P.Yu. (1997) Paleobiology of the late
892 Mesoproterozoic Sukhaya Tunguska Formation, Turukhansk Uplift, northestern
893 Siberia. *Precamb. Res*. **85**, 201-239.
894 Shields, G., and Veizer, J. (2002) Precambrian marine carbonate isotope database:
895 Version 1.1. *Geochemistry Geophysics Geosystems* **3**, 10.1029/2001GC000266.
896 Siever, R. (1991) Silica in the oceans: Biological-geochemical interplay, *in Scientists on*
897 *Gaia* (eds. S. Schneider and P. J. Boston), MIT press, pp. 287-295.
898 Siever, R. (1992) The Silica Cycle in the Precambrian. *Geochim. Cosmochim. Acta* **56**,
899 3265-3272.
900 Steinhoefel, G., Horn, I., and von Blanckenburg, F. (2009) Micro-scale tracing of Fe and
901 Si isotope signatures in banded iron formation using femtosecond laser ablation.
902 *Geochim. Cosmochim. Acta* **73**, 5343-5360.
903 Steinhoefel, G., von Blanckenburg, F., Horn, I., Konhauser, K.O., Beukes, N.J., and
904 Gutzmer, J. (2010) Deciphering formation processes of banded iron formations
905 from the Transvaal and the Hamersley successions by combined Si and Fe isotope
906 analysis using UV femtosecond laser ablation. *Geochim. Cosmochim. Acta* **74**,
907 2677-2696.
908 Strother, P.K., Knoll, A.H., and Barghoorn, E.S. (1983) Microorganisms from the Late
909 Precambrian Narssarssuk Formation, Northwestern Greenland. *Palaeontology* **26**,
910 1-32.
911 Tobin, K.J. (1990) The Paleoecology and Significance of the Gunflint-Type Microbial
912 Assemblages from the Frere Formation (Early Proterozoic), Nabberu Basin,
913 Western-Australia. *Precamb. Res.***47**, 71-81.

914 Tosca, N.J., Johnston, D.T., Mushegian, A., Rothman, D.H., and Knoll, A.H. (2010) Clay
915 mineralogy, organic carbon burial, and redox evolution in Proterozoic oceans.
916 *Geochim. Cosmochim. Acta* **74**, 1579-1592.
917 Treguer, P., Nelson, D.M., Vanbennekom, A.J., Demaster, D.J., Leynaert, A., and
918 Queguiner, B. (1995) The Silica Balance in the World Ocean - a Reestimate.
919 *Science* **268**, 375-379.
920 van den Boorn, S.H.J.M., van Bergen, M.J., Nijman, W., and Vroon, P.Z. (2007) Dual
921 role of seawater and hydrothermal fluids in Early Archean chert formation:
922 Evidence from silicon isotopes. *Geology* **35**, 939-942.
923 van den Boorn, S.H.J.M., van Bergen, M.J., Vroon, P.Z., de Vries, S.T., and Nijman, W.
924 (2010) Silicon isotope and trace element constraints on the origin of ~3.5 Ga
925 cherts: Implications for Earth Archaean marine environments. *Geochim.*
926 *Cosmochim. Acta* **74**, 1077-1103.
927 van den Boorn, S.H.J.M., Vroon, P.Z., van Belle, C.C., van der Wagt, B., Schwieters, J.,
928 and van Bergen, M.J. (2006) Determination of silicon isotope ratios in silicate
929 materials by high-resolution MC-ICP-MS using a sodium hydroxide sample
930 digestion method. *J. Anal. Atom. Spectrom.* **21**, 734-742.
931 Varela, D. E., Pride, C. J., and Brzezinski, M. A. (2004) Biological fractionation of
932 silicon isotopes in Southern Ocean surface waters. *Global Biogeochem. Cycles*
933 **18**, GB1047, doi:10.1029/2003GB002140.
934 Walter, M.R., Goode, A.D.T., and Hall, W.D.M. (1976) Microfossils from a newly
935 discovered Precambrian stromatolitic iron formation in Western Australia. *Nature*
936 **261**, 221-223.
937 Weyer, S., and Schwieters, J. (2003) High precision Fe isotope measurements with high
938 mass resolution MC-ICPMS. *Int. J. Mass. Spectrom.* **226**, 355-368.
939 Wilson, J.P., Fischer, W.W., Johnston, D.T., Knoll, A.H., Grotzinger, J.P., Walter, M.R.,
940 McNaughton, N.J., Simon, M., Abelson, J., Schrag, D.P., Summons, R., Allwood,
941 A., Andres, M., Gammon, C., Garvin, J., Rashby, S., Schweizer, M., and Watters,
942 W.A. (2010) Geobiology of the late Paleoproterozoic Duck Creek Formation,
943 Western Australia. *Precam. Res.***179**, 135-149.Ziegler, K., Chadwick, O.A.,
944 Brzezinski, M.A., and Kelly, E.F. (2005) Natural variations of delta Si-30 ratios

during progressive basalt weathering, Hawaiian Islands. *Geochim. Cosmochim. Acta* **69**, 4597-4610.

Li Yi-Liang, L., Konhauser, K. O., Cole, D. R. et al. (2011) Mineral ecophysiological data provide growing evidence for microbial activity in banded-iron formations. *Geology* **39**, 707-710 DOI: 10.1130/G32003.1.

Ziegler, K., Marin-Carbonne, J., McKeegan, K. D., and Young, E. D. (2011) Silicon and oxygen isotope values of cherts and their precursors. *Mineralogical Magazine* **75(3)**, 2284.

FIGURE CAPTIONS

Figure 1. Illustrative examples of cherts measured in this study, showing petrography and retention of micron scale features within cherts. Silicification occurred early in diagenesis, and the samples show little evidence for later diagenetic modification. A. Thin section of silicified lagoonal carbonate from the Akademikerbreen Group, Svalbard: silicified clasts, largely of microbial mats, are light brown; grey clasts and cements are dolomite; B and C, cyanobacterial microfossils preserved in early diageneticchert samples from the Akademikerbreen Group (B) and the Bil'yakh Group, Siberia. D. Bil'yakh chert showing preservation of depositional texture, most conspicuously, sub-mm scale aragonite crystals. Scale bar in C = 4 mm for A, = 20 microns for B, = 40 microns for C, and = 1 mm for D.

Figure 2. (a) Si isotopic composition of the cherts samples analyzed in this study as a function of their depositional age estimates. Open and filled blue symbols are peritidal cherts while blue crosses and pluses are cherts which formed by replacements of basinal carbonates. Red symbols are banded iron formations (BIF).

(b) All available bulk rock and in-situ MC-ICPMS data as well as in-situ ion-probe and SIMS results for cherts including our data (blue and red crosses). Data for Archean cherts are from Isua (BIFs, Andre et al., 2006), C and S cherts (van den Boorn et al., 2007, 2010), Onverwacht Group cherts (Abraham et al., 2011), Old Wanderer Formation BIFs

976 (Steinhoefel et al., 2009) and the Dales Gorge, Kuruman and Penge BIFs (Steinhoefel et
977 al., 2010). Error bars for all MC-ICPMS and SIMS data are smaller than the size of the
978 symbols. Ion probe data of Robert and Chaussidon (2006) are plotted with 2σ error bars
979 after correcting the ages of some of their samples based on more updated age estimates.
980 The ages have been corrected for samples from the Dengying Fm. (550Ma), Tindir Creek
981 (717-811 Ma), Pahrump Group (720-800 Ma), Amadeus Basin (800 Ma), Jixian Group
982 (1400-1600 Ma), McAurthur Basin (1590-1650 Ma), Nabberu Basin (1800 Ma), Wyllo
983 Group (1800-1900 Ma), Gunflint Fm. (1850-1900 Ma), Transvaal Basin (2500-2600 Ma),
984 Rietgat Fm. (2700 Ma), Keewatin Fm. (2700 Ma), and Manjeri Fm. (2700 Ma). The ion-
985 probe data of Robert and Chaussidon (2006) show a broadly similar temporal trend as the
986 MC-ICPMS data.
987
988 **Figure 3. (a)** A histogram of δ^{30}Si of cherts analyzed in this study plotted against the
989 frequency of samples. Red indicates basinal cherts associated with BIFs whereas blue
990 indicates non-BIF cherts.
991 **(b)** A compilation of all MC-ICPMS Si isotope data for Precambrian cherts including our
992 data. Literature data are from Isua (BIFs, Andre et al., 2006), Pilbara craton (C and S
993 cherts, van den Boorn et al., 2007, 2010), Onverwacht Group cherts (Abraham et al.,
994 2011), Old Wanderer Formation BIFs (Steinhoefel et al., 2009) and the Dales Gorge,
995 Kuruman and Penge BIFs (Steinhoefel et al., 2010). It is clear that BIFs typically show
996 lower δ^{30}Si compared to non-BIF cherts that were deposited in peritidal environments.
997
998 **Figure 4.** A simple isotope fractionation model showing open system (Rayleigh
999 fractionation) and closed system (equilibrium fractionation) variation of δ^{30}Si as a
1000 function of silica left in the residual solution (f). In the present context, the solution is
1001 silica saturated porewater (PW) while the precipitating solid are cherts. The δ^{30}Si of the
1002 initial porewater is taken as 0.8. In case 1, the Si isotope fractionation factor between PW
1003 (long-dashed lines) and cherts (solid lines) is assumed to be -2.0 ‰ and in case 2, it is
1004 taken as -3.0 ‰ (see text for details). Large δ^{30}Si variations in cherts from a single basin,
1005 as observed in the Spitsbergen cherts of the present study (~3.0 ‰), can be explained by
1006 Rayleigh-type fractionation with f ranging from 1 to 0.2 (grey and black arrows).

1007 Fractionations are much smaller for the equilibrium/closed-system scenario and require
1008 much lower values of f.

Table 1.

Sample #	Age (Ma)	Location	$\delta^{29}Si$	2SE	$\delta^{30}Si$	2SE	N	Other information (reference)
86P-121	750	Akademikerbreen Gr., Spitsbergen, Svalbard, Norway	-0.26	0.05	-0.51	0.06	3	Peritidal, silicified carbonate (1)
81P-4918	750	Akademikerbreen Gr., Spitsbergen, Svalbard, Norway	-0.90	0.03	-1.78	0.04	7	Peritidal, silicified carbonate (1)
81P-4705-2B	750	Akademikerbreen Gr., Spitsbergen, Svalbard, Norway	0.52	0.03	1.04	0.05	6	Peritidal, silicified carbonate (1)
86M-20-3	750	Akademikerbreen Gr., Spitsbergen, Svalbard, Norway	0.34	0.04	0.67	0.08	7	Peritidal, silicified carbonate (1)
81B-670	750	Akademikerbreen Gr., Spitsbergen, Svalbard, Norway	0.07	0.03	0.15	0.08	8	Peritidal, silicified carbonate (1)
81B-625-2A	750	Akademikerbreen Gr., Spitsbergen, Svalbard, Norway	-0.31	0.04	-0.62	0.07	7	Peritidal, silicified carbonate (1)
81B-550	750	Akademikerbreen Gr., Spitsbergen, Svalbard, Norway	-0.08	0.02	-0.14	0.06	9	Peritidal, silicified carbonate (1)
86P-96-2A	750	Akademikerbreen Gr., Spitsbergen, Svalbard, Norway	0.12	0.06	0.25	0.08	7	Peritidal, silicified carbonate (1)
86P-96	750	Akademikerbreen Gr., Spitsbergen, Svalbard, Norway	-0.22	0.05	-0.43	0.07	8	Peritidal, silicified carbonate (1)
86G-54-1	750	Akademikerbreen Gr., Spitsbergen, Svalbard, Norway	0.06	0.03	0.11	0.06	7	Peritidal, silicified carbonate (1)
81P-4353	750	Akademikerbreen Gr., Spitsbergen, Svalbard, Norway	-0.25	0.01	-0.48	0.03	6	Peritidal, silicified carbonate (1)
81P-4350-2	750	Akademikerbreen Gr., Spitsbergen, Svalbard, Norway	0.64	0.02	1.26	0.03	7	Peritidal, silicified carbonate (1)
86P-11-1	750	Akademikerbreen Gr., Spitsbergen, Svalbard, Norway	-0.35	0.04	-0.71	0.08	6	Peritidal, silicified carbonate (1)
86P-11-2	750	Akademikerbreen Gr., Spitsbergen, Svalbard, Norway	0.31	0.06	0.60	0.10	5	Peritidal, silicified carbonate (1)
81B-222	750	Akademikerbreen Gr., Spitsbergen, Svalbard, Norway	0.07	0.05	0.16	0.10	7	Peritidal, silicified carbonate (1)
86P-108-3	750	Akademikerbreen Gr., Spitsbergen, Svalbard, Norway	0.14	0.05	0.29	0.08	3	Peritidal, silicified carbonate (1)
81B-105-1A3	750	Akademikerbreen Gr., Spitsbergen, Svalbard, Norway	-0.69	0.04	-1.38	0.09	6	Peritidal, silicified carbonate (1)
SV-6	750	Akademikerbreen Gr., Spitsbergen, Svalbard, Norway	-0.01	0.05	-0.03	0.06	7	Peritidal, silicified carbonate (1)
SV-4	750	Akademikerbreen Gr., Spitsbergen, Svalbard, Norway	0.18	0.04	0.35	0.09	4	Peritidal, silicified carbonate (1)
81P-3400-3A	750	Akademikerbreen Gr., Spitsbergen, Svalbard, Norway	-0.30	0.02	-0.62	0.04	9	Peritidal, silicified carbonate (1)
81P-4077	750	Akademikerbreen Gr., Spitsbergen, Svalbard, Norway	-0.56	0.02	-1.14	0.05	7	Peritidal, silicified carbonate (1)
81P-5570	750	Akademikerbreen Gr., Spitsbergen, Svalbard, Norway	-0.33	0.05	-0.64	0.07	6	Peritidal, silicified carbonate (1)
T-714-1	770	Fifteenmile Gr., Alaska	-0.52	0.05	-1.03	0.06	8	Shallow subtidal, silicified carbonate (2)
T-714-2	770	Fifteenmile Gr., Alaska	-0.26	0.02	-0.51	0.03	7	Shallow subtidal, silicified carbonate (2)
E19-6-1	800	Limestone-Dolomite Series, east Greenland	-0.32	0.04	-0.61	0.08	8	Peritidal, silicified carbonate (3)
GR15-5	800	Limestone-Dolomite Series, east Greenland	-0.16	0.04	-0.32	0.07	8	Peritidal, silicified carbonate (3)
K1272	800	Hunnberg Fm., Nordaustlandet, Svalbard, Norway	0.00	0.04	-0.02	0.06	9	Peritidal, silicified carbonate (4)
K95-93	1000-1100	Sukhaya Tunguska Fm., NW Siberia	0.18	0.05	0.34	0.09	6	Peritidal, silicified carbonate (5)
K95-94	1000-1101	Sukhaya Tunguska Fm., NW Siberia	0.15	0.04	0.29	0.08	7	Peritidal, silicified carbonate (5)
K95-97	1000-1102	Sukhaya Tunguska Fm., NW Siberia	0.21	0.03	0.41	0.04	7	Peritidal, silicified carbonate (5)
K95-99	1000-1103	Sukhaya Tunguska Fm., NW Siberia	0.63	0.03	1.24	0.06	6	Peritidal, silicified carbonate (5)
K95-102	1000-1104	Sukhaya Tunguska Fm., NW Siberia	1.02	0.03	2.02	0.04	7	Peritidal, silicified carbonate (5)

Sample #	Age (Ma)	Location	$\delta^{29}Si$	2SE	$\delta^{30}Si$	2SE	N	Other information (reference)
KS78-21	1200	Narssarssuk Fm., NW Greenland	0.59	0.03	1.19	0.06	8	Peritidal, silicified carbonate (6)
KS78-1	1200	Narssarssuk Fm., NW Greenland	0.48	0.03	0.95	0.06	7	Peritidal, silicified carbonate (6)
KS78-2	1200	Narssarssuk Fm., NW Greenland	0.39	0.04	0.77	0.09	6	Peritidal, silicified carbonate (6)
KS78-5	1200	Narssarssuk Fm., NW Greenland	0.38	0.05	0.76	0.10	6	Peritidal, silicified carbonate (6)
KS78-12	1200	Narssarssuk Fm., NW Greenland	-0.31	0.06	-0.61	0.09	7	Peritidal, silicified carbonate (6)
KS78-14	1200	Narssarssuk Fm., NW Greenland	0.17	0.02	0.33	0.04	7	Peritidal, silicified carbonate (6)
KS78-15	1200	Narssarssuk Fm., NW Greenland	0.74	0.02	1.46	0.06	6	Peritidal, silicified carbonate (6)
KS78-18	1200	Narssarssuk Fm., NW Greenland	0.34	0.04	0.67	0.07	6	Peritidal, silicified carbonate (6)
A2-37855	1200	Society Cliffs Fm., Baffin Island, Canada	0.03	0.04	0.05	0.05	10	Peritidal, silicified carbonate (7)
WE 1740	1200	Society Cliffs Fm., Baffin Island, Canada	0.42	0.04	0.85	0.06	8	Peritidal, silicified carbonate (7)
KG-92-70	1450-1500	Yusmastakh Fm., Billyakh Gr., Siberia	0.91	0.03	1.81	0.04	12	Peritidal, silicified carbonate (8)
KG92-64-4A	1450-1500	Yusmastakh Fm., Billyakh Gr., Siberia	0.90	0.03	1.79	0.06	7	Peritidal, silicified carbonate (8)
KG92-60-2	1450-1500	Yusmastakh Fm., Billyakh Gr., Siberia	0.92	0.03	1.82	0.04	5	Peritidal, silicified carbonate (8)
KG92-57	1450-1500	Yusmastakh Fm., Billyakh Gr., Siberia	0.33	0.04	0.65	0.07	4	Peritidal, silicified carbonate (8)
KG92-59	1450-1500	Yusmastakh Fm., Billyakh Gr., Siberia	1.43	0.05	2.85	0.08	6	Peritidal, silicified carbonate (8)
KG92-61	1450-1500	Yusmastakh Fm., Billyakh Gr., Siberia	0.75	0.04	1.49	0.06	8	Peritidal, silicified carbonate (8)
KG92-67	1450-1500	Yusmastakh Fm., Billyakh Gr., Siberia	1.27	0.04	2.53	0.07	4	Peritidal, silicified carbonate (8)
KG92-30	1450-1500	Kotuikan Fm., Billyakh Gr., Siberia	0.06	0.03	0.11	0.05	9	Peritidal, silicified carbonate (8)
KG92-34	1450-1500	Kotuikan Fm., Billyakh Gr., Siberia	0.11	0.03	0.22	0.06	9	Peritidal, silicified carbonate (8)
KG92-40	1450-1500	Kotuikan Fm., Billyakh Gr., Siberia	-0.11	0.02	-0.20	0.04	7	Peritidal, silicified carbonate (8)
KG92-47	1450-1500	Kotuikan Fm., Billyakh Gr., Siberia	0.07	0.03	0.13	0.05	7	Peritidal, silicified carbonate (8)
F-1	1800	Frere Fm., W Australia	-1.35	0.08	-2.68	0.15	6	Oolitic IF (9)
DCC37	1880	Duck Creek Fm., W Australia	-0.94	0.02	-1.86	0.05	9	Basinal, associated with IF (10)
DCC10	1880	Duck Creek Fm., W Australia	-2.15	0.05	-4.29	0.07	6	Basinal, associated with IF (10)
DC08	1880	Duck Creek Fm., W Australia	-0.79	0.03	-1.57	0.06	7	Basinal, associated with IF (10)
DC38	1880	Duck Creek Fm., W Australia	-0.95	0.03	-1.91	0.05	7	Basinal, associated with IF (10)
GF70-32	1880	Gunflint Fm., Canada	-0.49	0.02	-1.01	0.04	10	Stromatolitic IF (11)
GF66-3a	1880	Gunflint Fm., Canada	-0.42	0.05	-0.82	0.09	6	Basinalchert, with siderite (11)
B-1	1880	Biwabik Fm., Minnesota, USA	-0.71	0.06	-1.42	0.10	7	Hematiticstromatoilitic IF (12)

Sample #	Age (Ma)	Location	$\delta^{29}Si$	2SE	$\delta^{30}Si$	2SE	N	Other information (reference)
A68-10	2500	Brockman Fm., Hamersley Gr. Australia	-0.31	0.05	-0.61	0.08	6	Banded IF (13)
A68-2	2570	Wittenoom Fm., Hamersley Gr. Australia	-0.55	0.03	-1.11	0.04	8	Chert in basinal dolomite (13)
P7	2530	Griqualand West, Transvaal SG., S Africa	0.17	0.05	0.33	0.10	5	Basinal, BIF (14)
P21	2530	Griqualand West, Transvaal SG., S Africa	0.26	0.05	0.51	0.11	4	Basinal, BIF (14)
GKF 896.14	2530	Griqualand West, Transvaal SG., S Africa	-0.55	0.03	-1.11	0.06	6	Basinal, BIF (14)
GKF 896.34	2530	Griqualand West, Transvaal SG., S Africa	0.29	0.05	0.57	0.08	8	Basinal, BIF (14)
GKF 896.47	2530	Griqualand West, Transvaal SG., S Africa	0.15	0.03	0.28	0.05	4	Basinal, BIF (14)
GKF 897.26	2530	Griqualand West, Transvaal SG., S Africa	-0.35	0.03	-0.71	0.06	9	Basinal, BIF (14)
Ga13	2530	Griqualand West, Transvaal SG., S Africa	0.14	0.02	0.26	0.05	6	Basinal, shale and calcite (14)
Ga17	2530	Griqualand West, Transvaal SG., S Africa	-0.16	0.03	-0.31	0.06	7	Basinal, shale and calcite (14)
Whr 30.1	2530	Griqualand West, Transvaal SG., S Africa	0.71	0.04	1.41	0.08	7	Basinal, shale and calcite (14)
MonT. 450m	2530	Griqualand West, Transvaal SG., S Africa	0.09	0.05	0.20	0.08	6	Peritidal dolomite (14)
Kg10	2530	Griqualand West, Transvaal SG., S Africa	0.91	0.02	1.81	0.04	7	Peritidal dolomite (14)
Kg20	2530	Griqualand West, Transvaal SG., S Africa	0.74	0.04	1.48	0.08	5	Peritidal dolomite (14)

Table 1. Stable Si isotope data for 2570-750 Ma old cherts analyzed in this study from different geographic locations. The uncertainty for $\delta^{29}Si$ and $\delta^{30}Si$ measurements are given as $2\sigma_m$ and N denotes the number of repeat measurements.Also shown are available information on the depositional facies and precursor rock type. References describing detailed sedimentology and petrography of these samples are as follows: 1. Knoll et al. 1989,1991; 2. Allison and Awramik, 1989; Macdonald et al., 2010, 2011; 3. Green et al., 1989; 4. Knoll, 1984; 5. Sergeev et al. 1997; 6. Strother et al., 1983; 7. Kah and Knoll, 1996; 8. Sergeev et al., 1995; 9. Walter et al., 1976, Tobin, 1990; 10. Wilson et al., 2010; 11.Barghoorn and Tyler 1965; 12.Brotton et al., 2007; 13.Yi-Liang et al., 2011; 14.Knoll and Beukes, 2009, Fischer and Knoll, 2009.

Table 2. A compilation of estimated Si concentrations and fluxes to the modern and Precambrian oceans as well as the isotopic compositions (δ^{30}Si) of modern seawater, igneous rocks, and hydrothermal and continental fluxes of Si to the modern ocean. Also listed are the isotopic fractionation factors (Δ^{30}Si) between seawater and diatoms[1], seawater and sponges[2], diatoms and fluids (after diatom dissolution) [3],Si rich fluid and silica adsorbed on to Fe hydroxides[4], and quartz and kaolinite[5]. Note that both biologically and physically precipitated silica preferentially incorporates lighter Si isotopes. See text for details.

	Modern Ocean	**Precambrian Ocean**
Average Si concentration	2 ppm (<1 ppm to 15 ppm)	120-140 ppm
Continental influx of Si	5.5 $\pm$ 1.2 Tmoles/year	
Marine/Hydrothermal influx of Si	0.6 $\pm$ 0.3 Tmoles/year	
Biological outflux of Si	7.1 $\pm$ 1.8 Tmoles/year	
Residence time of Si	~15,000 years	0.9 - 1.05 Ma
Average δ^{30}Si (modern seawater)	1.1	
δ^{30}Si (igneous rocks)	-0.39	
δ^{30}Si (hydrothermal flux to modern sw)	-0.4	
δ^{30}Si (continental flux to modern sw)	0.8	
Δ^{30}Si (seawater - diatoms)[1]	1.1	
Δ^{30}Si (seawater - sponges)[2]	3.5	
Δ^{30}Si (diatoms - fluid)[3]	0.55	
Δ^{30}Si (fluid - silica adsorbed onto Fe hydroxides)[4]	1.1 to 1.6	
Δ^{30}Si (quartz - kaolinite)[5]	1.6	

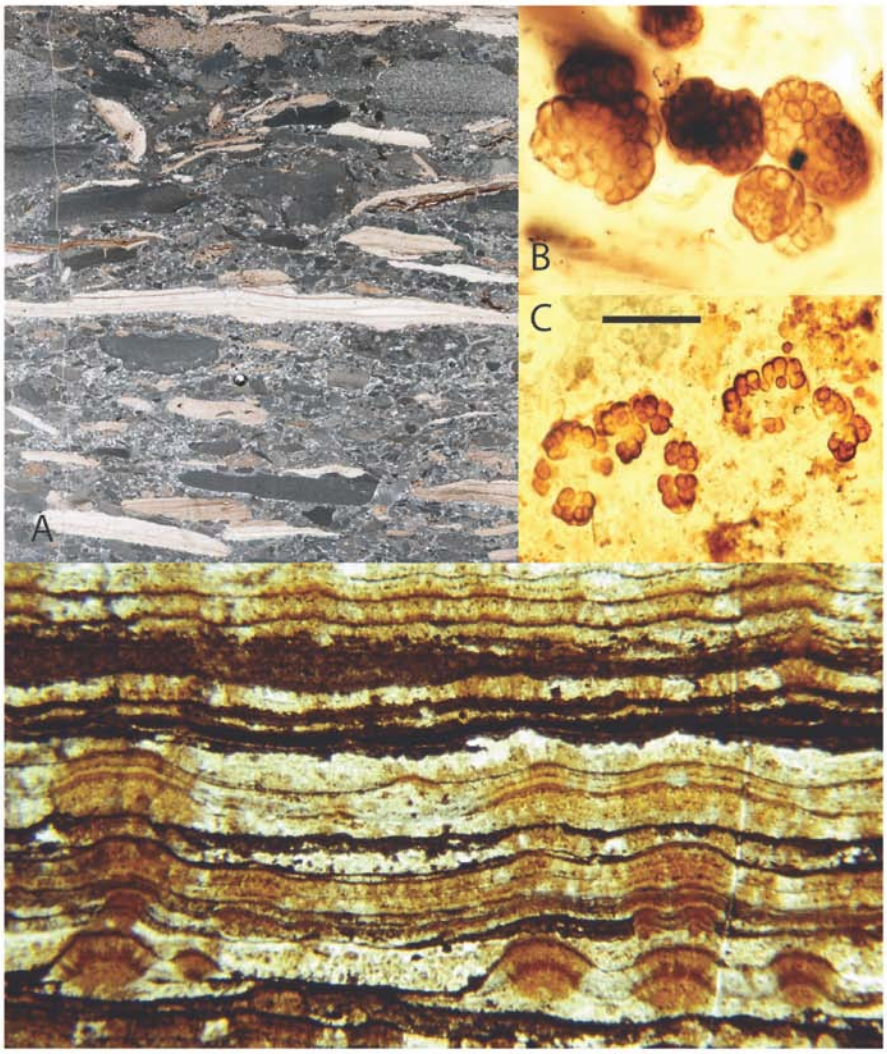

Figure 1.

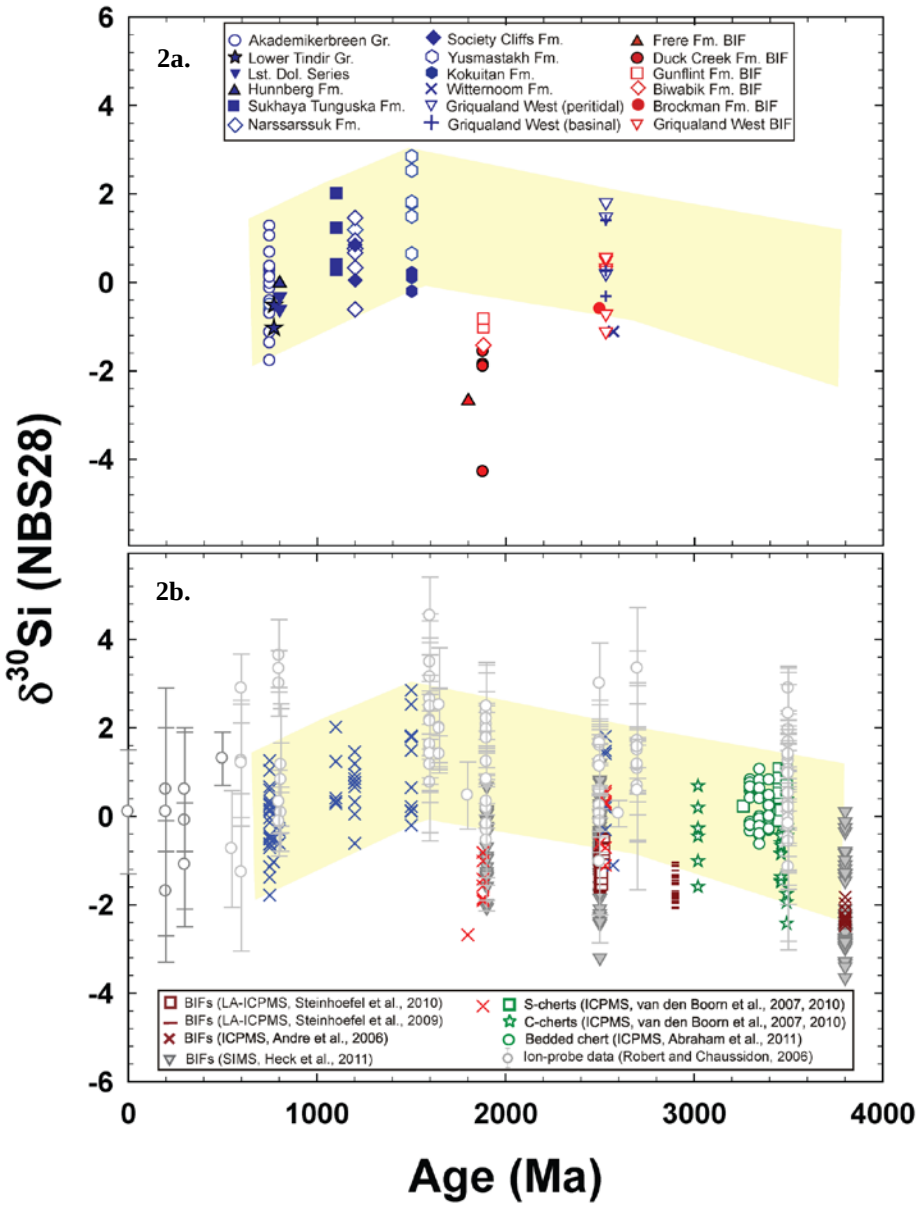
2a.
Akademikerbreen Gr.
Lower Tindir Gr.
Lst. Dol. Series
Hunnberg Fm.
Sukhaya Tunguska Fm.
Narssarssuk Fm.
Society Cliffs Fm.
Yusmastakh Fm.
Kokuitan Fm.
Wittenoom Fm.
Griqualand West (peritidal)
Griqualand West (basinal)
Frere Fm. BIF
Duck Creek Fm. BIF
Gunflint Fm. BIF
Biwabik Fm. BIF
Brockman Fm. BIF
Griqualand West BIF
2b.
BIFs (LA-ICPMS, Steinhoefel et al., 2010)
BIFs (LA-ICPMS, Steinhoefel et al., 2009)
BIFs (ICPMS, Andre et al., 2006)
BIFs (SIMS, Heck et al., 2011)
S-cherts (ICPMS, van den Boorn et al., 2007, 2010)
C-cherts (ICPMS, van den Boorn et al., 2007, 2010)
Bedded chert (ICPMS, Abraham et al., 2011)
Ion-probe data (Robert and Chaussidon, 2006)
δ30Si (NBS28)
Age (Ma)
6
4
2
0
-2
-4
-6
0
1000
2000
3000
4000

Figure 2.

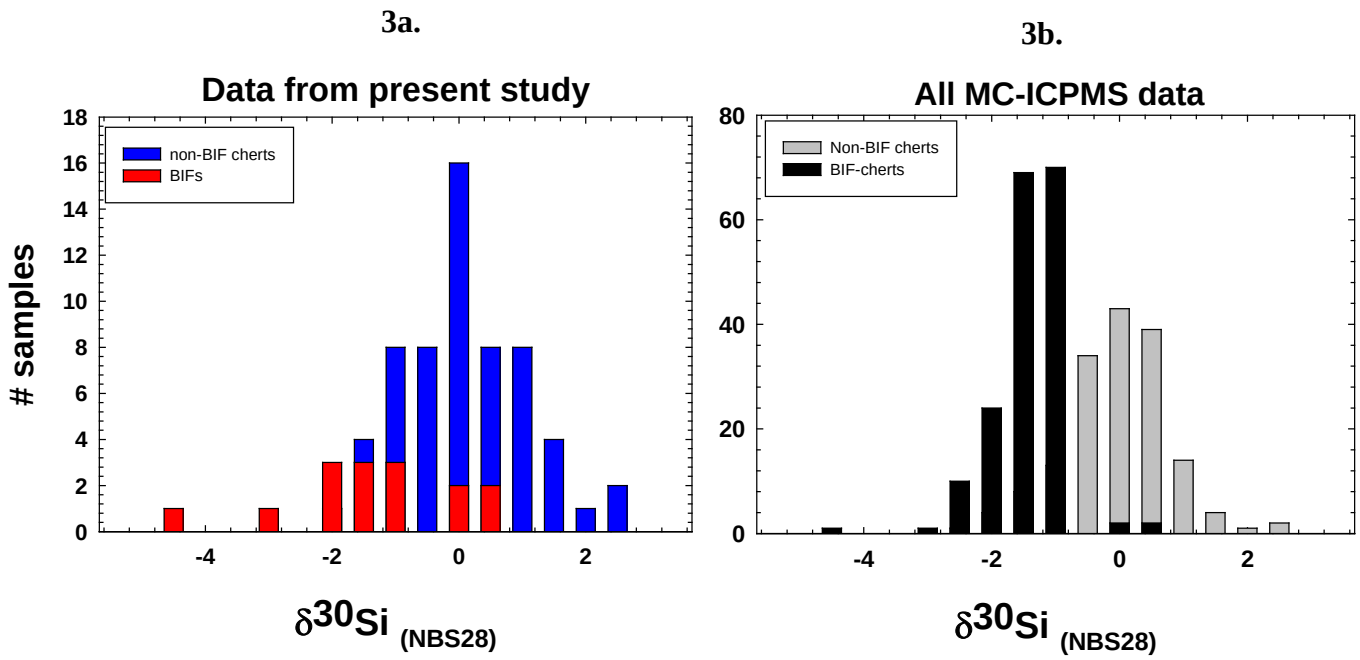
3a.
Data from present study
non-BIF cherts
BIFs
samples
δ30Si (NBS28)
3b.
All MC-ICPMS data
Non-BIF cherts
BIF-cherts
δ30Si (NBS28)

Figure 3.

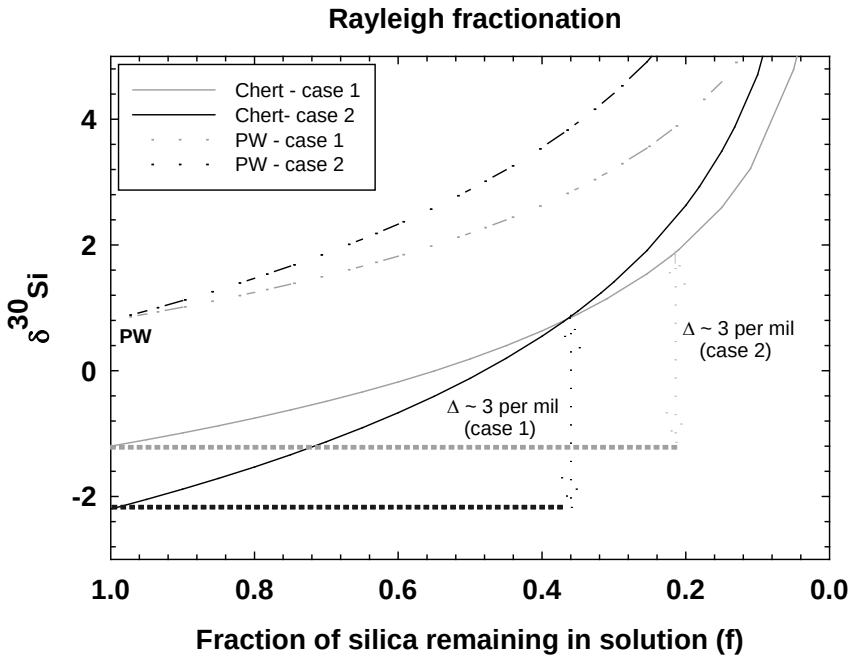
Rayleigh fractionation
Chert - case 1
Chert- case 2
PW - case 1
PW - case 2
PW
Δ ~ 3 per mil
(case 2)
Δ ~ 3 per mil
(case 1)
δ30Si
4
2
0
-2
1.0
0.8
0.6
0.4
0.2
0.0
Fraction of silica remaining in solution (f)

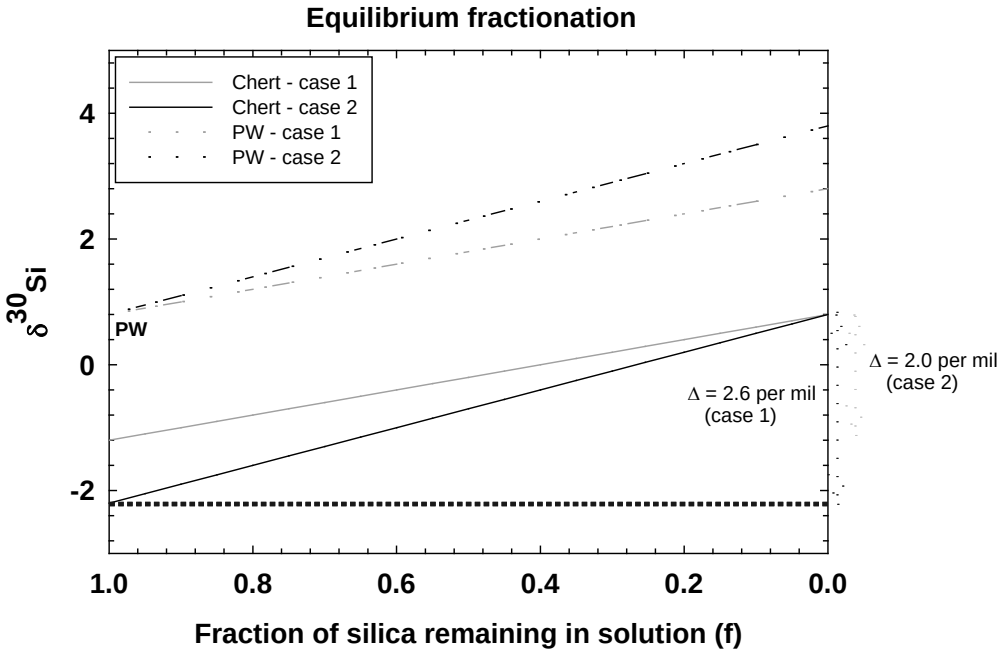
Equilibrium fractionation
Chert - case 1
Chert - case 2
PW - case 1
PW - case 2
PW
Δ = 2.6 per mil
(case 1)
Δ = 2.0 per mil
(case 2)
δ30Si
4
2
0
-2
1.0
0.8
0.6
0.4
0.2
0.0
Fraction of silica remaining in solution (f)

Figure 4.